https://doi.org/10.5194/egusphere-2026-3251
Preprint. Discussion started: 23 June 2026

The Madden Julian Oscillation in high-resolution coupled climate simulations: mean state evaluation and historical variability in IFS-NEMO

Bernardo Maraldi[1,3], Nuno Rocha Monteiro[1], Marvin Axness[1], Daria Kuznetsova[1], Pablo Ortega[1], Francisco Doblas-Reyes[1,2]
[1]Barcelona Supercomputing Center, (BSC), Barcelona, Spain
[2]ICREA, Barcelona, Spain
[3]Universitat de Barcelona, Barcelona, Spain

Correspondence to: Bernardo Maraldi (bernardo.maraldi@bsc.es)

Abstract. This work examines the representation of the MJO in two high-resolution versions of the fully coupled General Circulation Model IFS-NEMO, a new-generation climate model developed at the BSC within the European Project EERIE and the Destination Earth initiative. We analyse two historical HighResMIP simulations of IFS-NEMO performed at two different horizontal resolutions: 9 km and 25 km, to investigate the impact of the resolution on MJO performance. The model correctly reproduces the main dynamical features associated with the MJO when defined via multivariate EOF analysis, and exhibits typical model biases. The model correctly reproduces the spatial properties of the two leading observed EOFs, but the mean amplitude of the MJO and the intensity of the convective signal are generally underestimated, with a reduction of spectral power of about 20% at both resolutions with respect to satellite observations. IFS-NEMO also exhibits a reduced eastward propagation of the intraseasonal precipitation and convective signals associated with the MJO. This is explained by the strong dry bias found in the early phases of the MJO (over the Indian Ocean) in both versions of IFS-NEMO with respect to ERA5. Low-atmospheric moistening is crucial during those phases as moisture accumulation drives both vertical and horizontal humidity advection. Overall, the 10 Km configuration seems to improve the structure of the two leading EOFs and their explained variance, without solving the other biases. The simulations do not reproduce the long-term change of MJO activity observed over the full historical period. In particular, the MJO variance increases in observations, while none of the IFS-NEMO simulations shows a significant trend. This is due to cold ocean and background circulation biases. Finally, the implications that such a discrepancy can have on predictability are discussed by analysing the changes in weighted permutation entropy of the MJO amplitude time series. Contrary to ERA5, the predictability does not increase in IFS-NEMO at both resolutions, as the model fails to reproduce the externally forced predictive component of the MJO, thus questioning their suitability to investigate the projected future evolution.

https://doi.org/10.5194/egusphere-2026-3251
Preprint. Discussion started: 23 June 2026

1 Introduction

The Madden Julian Oscillation (MJO) is one of the main modes of intraseasonal climate variability in the Tropics. First identified by Madden and Julian (1971), the MJO is a phenomenon characterised by organised convective systems coupled to the atmospheric circulation. It involves an eastward-propagating convective center, which develops over the warm pool of the Indian Ocean and dissipates as it reaches the Central-Eastern Tropical Pacific, preceded by an analogous region of suppressed convection at its eastward end, establishing an oscillation that recurs on timescales from 30 to 80 days. This system can modulate the El Niño–Southern Oscillation (ENSO), triggering some positive ENSO events (Kessler and Kleeman, 2000), and has also been shown to influence the Indian and Australian monsoons (M. C. Wheeler et al., 2009; Taraphdar et al., 2018), tropical cyclone activity (Fowler and Pritchard, 2020) and many other climate phenomena worldwide through atmospheric circulation perturbations (Vitart, 2017; Stan et al., 2022; Yadav et al., 2024). Tightly coupled to the large-scale atmospheric circulation, the MJO constitutes the largest single source of predictability for the climate both in the Tropics and in the extra-tropics on the subseasonal to seasonal (S2S) timescale (Stan et al., 2017).

A good representation of the MJO is therefore crucial for forecast models to enhance their prediction skill. Considerable efforts have been devoted by multiple groups around the world (Vitart et al., 2017) to identify and correct common deficiencies of both weather forecast models and General Circulation Models (GCMs) in representing the MJO, with the focus often put on unifying diagnostic procedures to evaluate the model's behaviour (Waliser et al., 2009). Applications to fully coupled GCMs have shown improvement in the course of the years through increases in horizontal resolution and better convection parametrization, allowing models from the Coupled Model Intercomparison Project phase 6 (CMIP6) to generally outperform their CMIP5 predecessors (Waliser et al, 2009; Ahn et al., 2020). Ocean–atmosphere coupling has emerged as an important factor in this progress: interactive SSTs improve the coherence and propagation speed of the simulated MJO compared to atmosphere-only configurations, particularly through the rectifying effect of air-sea heat fluxes ahead of the convective envelope (Klingaman and Woolnough, 2014; DeMott et al., 2015). Despite these improvements, GCMs still struggle to reproduce key aspects of the observed MJO variability, presenting systematic biases in its amplitude, propagation speed and coherence, with the Maritime Continent barrier – a tendency of models to suppress MJO convection as it crosses the Indonesian archipelago – remaining one of the most documented deficiencies across model generations (Ahn et al., 2020; Jiang et al., 2020; Merryfield et al., 2020).

Wheeler and Hendon (2004) established a standard procedure to monitor MJO activity, providing a seasonally independent characterization of its state through the Realtime Multivariate MJO (RMM) indices, which are commonly applied in the S2S prediction community. However, recent studies have illustrated the sensitivity of MJO activity diagnostics and model prediction skill metrics to the index of choice (H. Kim et al., 2018; Liu et al., 2016; Lyu et al., 2019; Stachnik and Chrisler, 2020), comparing the RMM approach against single-variable alternatives, such as the Outgoing longwave radiation-based MJO Index (OMI; Kiladis et al., 2014), or the velocity potential index (Ventrice et al., 2013), each carrying distinct advantages and limitations in terms of noise sensitivity, physical interpretability and seasonal dependence.

https://doi.org/10.5194/egusphere-2026-3251
Preprint. Discussion started: 23 June 2026

The index choice is also important for exploring the long term variability of the MJO and its response to climate change, as shown by Lyu et al. (2019), who compared the RMM, OMI and relative variations. Differences in the long-term changes in the MJO have also been reported between different reanalysis datasets (Dias et al., 2025). Such a heterogeneity of methods and perspectives, in spite of numerous efforts of standardization, still leads to heterogeneous conclusions (Lyu et al., 2019; Maloney et al., 2019; Weidman et al., 2022).

These methodological challenges become especially relevant as climate modelling enters the era of storm-resolving global models. Much of the literature on MJO simulation and long-term variability has relied on conventional-resolution GCMs. Some studies have previously highlighted the impacts of explicit convection and storm-resolving resolutions on the MJO representation in models, but limited by reduced spatial or temporal domains (Miura et al., 2007; Holloway et al., 2013). The advent of eddy-permitting and eddy-resolving coupled models opens new opportunities to address some persistent deficiencies. Higher atmospheric resolution can improve the representation of mesoscale convective organisation, sharpen topographic forcing over the Maritime Continent (Jiang et al., 2019), and resolve finer oceanic structures (Roberts et al., 2026) that feed back onto the atmospheric boundary layer — all processes known to influence MJO propagation.

The scope of this paper is to investigate the impact of horizontal resolution on the representation of the MJO in two different configurations of the global coupled GCM IFS-NEMO at eddy-permitting (~25 km) and eddy-resolving (~9 km) resolution, evaluating their performance against observational and reanalysis benchmark. The paper additionally examines long-term MJO variability, as captured by the RMM index, and its sensitivity to the choice of the reference period, extending the recent work of Dias et al. (2025). This evaluation allows us to identify the strengths and the shortcomings of its eddy-resolving configuration, which is currently being used at the Earth Sciences Department of the Barcelona Supercomputing Center (BSC) to implement a new generation seasonal-to-decadal (S2D) climate prediction system.

The paper is organised as follows. Section 2 describes the GCM, the simulations performed and the validation data, as well as the methodologies employed to characterize and evaluate the MJO. Most metrics used here are well known and have been widely used in recent years of research on the MJO. Section 3 presents the results of the model evaluation with a particular focus on the impact of horizontal resolution on the different metrics. Section 3 also explores the sensitivity of the commonly used RMM index to the choice of the reference period as well as its length. Finally, section 4 summarizes our findings and sets the foundations for the upcoming application of IFS-NEMO to investigate the potential predictability of the MJO, building on the strengths, shortcomings and caveats discussed in the other sections.

2 Data and methods

2.1 Model and experiment description

The current work is based on the analysis of two historical simulations performed with IFS-NEMO at two different horizontal resolutions. IFS-NEMO is a new generation fully coupled GCM specifically developed within the Destination

https://doi.org/10.5194/egusphere-2026-3251
Preprint. Discussion started: 23 June 2026

Earth initiative (Doblas-Reyes et al., 2026) and the European project EERIE for km-scale climate modeling. The model combines version 4.0.7 of the ocean model NEMO (Gurvan et al., 2019) with an EERIE-revised build of cycle 48r1 of the atmospheric model IFS (DE_CY48R1.0_EERIE_20240726). The sea-ice model SI3 (Vancoppenolle et al., 2023) is integrated within NEMO and runs on the same ocean grid, ensuring consistent representation of ice–ocean thermodynamic and dynamical interactions. We use an eddy-rich configuration (IFS-NEMO-ER) with an atmospheric resolution of ~9 km (based on a Tco1279 Gaussian octahedral grid) and an ocean at 1/12° resolution (based on an eORCA12 tripolar global curvilinear grid), and a lower-resolution configuration (IFS-NEMO-HR) with a ~25 km atmosphere (Tco399) and a 1/4° ocean (eORCA025). In both configurations, the atmosphere is discretized with 137 vertical levels, while the ocean uses 75 vertical levels. The three components are coupled through a single executable approach (Mogensen et al. 2012), allowing them to run together using a common time step loop. This tightly integrated setup enables highly efficient, low-latency data exchange, which is critical for high-resolution, fully coupled simulations. The coupling operates at a 1-hour frequency, exchanging essential fields – such as sea surface temperature (SST), surface fluxes, ice cover, and ocean currents – between IFS and NEMO to capture dynamic interactions among the atmosphere, ocean, and sea ice.

The simulations performed with IFS-NEMO-HR and IFS-NEMO-ER extend from 1950 to 2014, and correspond to hist-1950 experiments from the High Resolution Model Intercomparison Project (Haarsma et al., 2016). Both are initialized from 60-year long spin-up experiments with fixed 1950 forcing. For the sake of this analysis, and following common practice, when it comes to MJO diagnostics both model and validation data have been previously regridded onto a common 2.5º by 2.5º horizontal grid.

2.2 Validation datasets

The reanalysis product ERA5 from ECMWF (Hersbach et al., 2020) was used as our primary reference to evaluate the model performance. ERA5 provides observationally constrained, physically consistent meteorological fields and shares IFS as its underlying atmospheric component with the two model versions of IFS-NEMO evaluated — albeit at a different version — making it a particularly coherent benchmark for assessing the model performance. For outgoing longwave radiation (OLR), however, we used a daily satellite-based product provided by NOAA (Liebmann and Smith, 1996), as OLR in ERA5 is diagnosed by the model and not directly assimilated from observations. This product comes on a 2.5º by 2.5º horizontal regular grid and is available continuously from 1979 to present. Our main validation is focused on 1979-2014, the overlapping period between ERA5, the observations and the IFS-NEMO historical simulations. We hereinafter refer to the validation dataset as ERA5-NOAA for the 1979-2014 period. The RMM index, a season-independent metric defined by Wheeler and Hendon (2004) to track the activity of the MJO, was also used for validation and are provided by the Australian Meteorological Bureau at http://www.bom.gov.au/climate/mjo/graphics/rmm.74toRealtime.txt. ERA5 has been used as reference also for the validation of the long term variability analysis over the period 1950-2014.

https://doi.org/10.5194/egusphere-2026-3251
Preprint. Discussion started: 23 June 2026

2.3 MJO diagnostics

Focusing on different levels of diagnostics such as those introduced by (M. Wheeler and Kiladis 1999; M. C. Wheeler and Hendon, 2004; Waliser, 2009) the main variables used for our analysis are the zonal wind speed at 850 hPa (ua850) and 200 hPa (ua200), outgoing longwave radiation at the top of the atmosphere (OLR), precipitation (pr), specific humidity (hus) and sea surface temperature (SST).

2.3.1 EOF characterization

To monitor the MJO, this study leverages the methodology introduced by Wheeler and Hendon (2004), hereinafter WH04. WH04 introduced a procedure that applies an empirical orthogonal function (EOF) analysis to a combined (multivariate) dataset of tropically (15º S–15º N) averaged zonal wind speed at 850 hPa and 200 hPa (ua850, ua200), and outgoing longwave radiation (OLR) fields. The first two principal components of the analysis are used as RMMs. Since it does not require filtering, the WH04 approach is the most suitable for realtime applications (Gottschalck et al., 2010; Rashid et al., 2011; Vitart, 2017). It is also predominantly used to investigate long-term MJO variability (Cui and Li, 2022; Dias et al., 2025; H.-R. Kim et al., 2025). For this reason, we adopted the methodology of WH04, neglecting the ENSO-related variability removal step, as described by Gottschalck et al. (2010).

For the main validation period the EOF analysis is performed with ERA5 wind fields and OLR from NOAA satellite dataset. To assess the sensitivity of the MJO to the OLR source, we carried out an additional computation that uses both radiation and wind fields from ERA5 (i.e., referred to hereinafter as ERA5). This ERA5-based computation was also applied to earlier periods using sliding 35-year temporal windows with one-year increments until the beginning of the simulated period (i.e. 1950), which has allowed us to investigate the multi-decadal variability of the MJO amplitude and phase, similarly to the analysis of Dias et al. (2025). We note that while Dias et al. (2025) state that the length of the window has no qualitative impact on the MJO evolution over time, our longer 35-year window has been found to reduce uncertainty in the computed EOFs, which are more consistent over time. The following different approaches have been considered in the computation of the RMMs to investigate the long-term variability in the MJO:

- Computing the EOFs as in WH04 separately for each dataset (simulations and ERA5) and sliding window. The main benefit of this method is that the real features of the intraseasonal variability contained in each multivariate subset can be extracted, together with the corresponding variance associated with the first two eigenvectors. However, the RMM-like indices obtained through this procedure cannot be compared across different windows and datasets as the normalization happens independently and the principal components effectively differ, implying that they do not represent the same modes over time.
- Projecting the simulated intraseasonal ua850, ua200 and OLR anomalies onto present-day (i.e. 1979-2014) EOFs derived from ERA5-NOAA to evaluate how the models represent this fixed representation of the reanalysed MJO over time. This approach yields two new time series that correspond to the RMMs defined by WH04. We

https://doi.org/10.5194/egusphere-2026-3251
Preprint. Discussion started: 23 June 2026

additionally "reconstruct" the simulated ua850, ua200 and OLR anomalies by projecting the RMMs thus derived for each dataset onto the same set of EOFs. Such datasets contain the MJO variability as described by the present-day observed EOF. The fraction of variance in the reconstructed dataset can be compared with the one retrieved by the EOF analysis (sum of the first two eigenvalues). This methodology ensures that the long term analysis is consistent for each dataset individually. However, the first two EOFs differ between ERA5 and IFS-NEMO.

- Finally, we performed a complementary analysis by reconstructing each multivariate dataset using the present-day EOFs derived from that same dataset (i.e., ERA5-derived EOFs for the ERA5 data and IFS-NEMO-derived EOFs for the IFS-NEMO data).

Finally, lag correlations between the first two principal components computed from the EOF analysis on each dataset respectively are used to evaluate their mutual coupling and its influence on the dominant temporal scale of the MJO. Since these components form a pair in quadrature with an approximate phase difference of 90º, the lag at which the maximum correlation occurs provides an estimate of the periodicity of the MJO.

2.3.2 MJO propagation in space and time

For this diagnostic, we first applied a 30-80 day bandpass filter, following previous studies (Waliser, 2009; H.-R. Kim et al., 2025). To investigate how MJO-driven OLR anomalies propagate in time and space, we then computed lag-longitude diagrams showing the correlation of boreal winter (i.e., December to February or DJF) for OLR and ua850 with the corresponding average in a reference region over the Indian Ocean (15º S-10º N, 75º E-100º E). While using averages over a large box rather than a single point induces smaller correlation values, this box-average was found to be more suitable to track the actual propagating signal. Additionally, we computed the propagation speed by identifying consecutive correlation maxima at each longitudinal grid point, considering only correlations exceeding a significance threshold of 0.3, using a similar approach to Kim et al. (2025). We then computed the propagation speed as the slope of a linear fit using a least-square method. We observed that extracting the propagation speed with this procedure is sensitive to the arbitrary choice of the significance correlation threshold. Different choices have been found to yield different propagation speeds and could lead to different conclusions. We therefore include an uncertainty estimate obtained from bootstrapping 1000 times the lag-lon pairs — the ones used for the linear fit — allowing for repetition. To improve comparison with reanalysis data, the minimal common longitudinal interval across the three datasets with significant correlations was selected. The significance of the correlation was computed using a Student's t-test and correcting the number of degrees of freedom for autocorrelation in the time series (Zwiers and Von Storch, 1995; Afyouni et al., 2019).

A complementary method to investigate the spatio-temporal aspects of MJO propagation is to compute composite maps of MJO-relevant anomalies for each MJO phase. These phases are defined from the joint evolution of the two leading principal components, whose normalized amplitudes span a two-dimensional phase space. The instantaneous MJO phase is determined by the angle in this phase space, while its amplitude is given by the radial distance from the origin, thereby defining the canonical eight-phase MJO life cycle. To evaluate the propagation of convective signals associated with the

https://doi.org/10.5194/egusphere-2026-3251
Preprint. Discussion started: 23 June 2026

MJO, we produced composite maps of precipitation and specific humidity subseasonally filtered anomalies for each phase of the MJO (Wheeler and Hendon, 2004; Cao et al., 2025). The composites of the different phases were then built by averaging all the active days (i.e. the amplitude $A = \sqrt{PC_1^{\,2} + PC_2^{\,2}} > 1$) belonging to each respective phase. The composite selection is sensitive to the methodology used to retrieve the RMMs. We computed the composites by deriving the RMMs from projections of the multivariate anomalies onto either a fixed set of EOFs derived from ERA5–NOAA or EOFs computed separately for each dataset (as described in Section 2.3.1). The statistical significance of the composites is computed by selecting the 99 % level from a bootstrapped distribution of a randomly extracted subsample of all the available days, with the same size of the one used for the composite and allowing for repetitions.

2.3.3 MJO spectral properties

The symmetric wavenumber-frequency power spectrum of OLR was computed, following the steps first introduced by M. Wheeler and Kiladis (1999). The methodology involves filtering the spectra by removing a red-noise background obtained for each dataset independently by smoothing the raw spectra an arbitrary amount of times both in the wavenumber and in the frequency domain. Raw spectra are computed on consecutive 96-day segments that overlap for 60 days and averaged. Finally, power is summed for all latitudes between 15º S and 15º N. The significant peaks are identified at a 95 % confidence level of an F-distribution. The total number of degrees of freedom (dof), which can be derived by counting the number of independent 96 over the entire period (1979-2014), is about 1600 (35*365*12/96). Considering that all segments are not truly independent due to the 60-day overlap, a more conservative estimate yields approximately 1,000 dof. To quantify the differences between IFS-NEMO and observations in terms of MJO spectral power, we computed the averaged ratio between the simulated and the observed power spectra in the intervals from 1/30 to 1/80 days^{-1} for frequency and from 1 to 4 for wavenumbers (Chang et al., 2020).

2.3.4 Walker Circulation and Indo-Pacific Warm Pool

We characterised the mechanisms responsible for the long term evolution of the MJO activity by investigating the multidecadal changes in the Walker Circulation (WC) and the Indo-Pacific Warm Pool (IPWP). We employed a WC index based on the sea level pressure difference between an Eastern Box (5º S–5º N, 160º–80º W) and Western Box (5º S–5º N, 80º–160º E) of the Pacific ocean as defined by Kociuba and Power (2015). Additionally, the long term changes in the IPWP have been evaluated in terms of both its total spatial extension and intensity. The IPWP area is defined as the tropical region with sea surface temperatures above the 28 ºC isotherm between the Indian Ocean and the Western Pacific, considered here as the 25° S to 25° N and 40° E to 130° W box. The intensity is the area weighted average within this region (Weller et al., 2016). All data used for this analysis have been previously interpolated to a 1º by 1º horizontal grid.

https://doi.org/10.5194/egusphere-2026-3251
Preprint. Discussion started: 23 June 2026

2.3.6 Weighted Permutation Entropy

Weighted Permutation Entropy (WPE) is a measure that quantifies the complexity of a time series. Specifically, WPE leverages on the concept of entropy introduced by Shannon (1948) in the context of information theory. Bandt and Pompe (2002) extended the idea by defining permutation entropy as a tool to classify time series on the basis of the frequency with which certain patterns (ordinal patterns) recur throughout the timeseries (Leyva et al., 2022). WPE replaces the traditional permutation entropy definition by using occurrence frequencies that are weighted according to the variance of the selected ordinal patterns. A time series dominated by a small number of recurring ordinal patterns has low entropy and low complexity, meaning that its future evolution is more constrained and therefore more predictable; conversely, a high-entropy series is more random and less predictable. We therefore use WPE as a proxy for MJO predictability, with decreasing entropy over time indicating that the MJO is becoming a more regular and predictable mode of variability. For mathematical details, we refer to Du et al. (2024) who were the first ones to apply WPE to study the MJO predictability. We employ the same technique here to investigate the long term changes in the predictability of MJO associated with the RMMs amplitude.

3. Results

3.1 MJO evaluation over the most recent period

This first part of the results section focuses on the 1979-2014 period, for which the direct OLR observations from NOAA are available and ERA5 assimilates higher quality and more widespread observations.

Figure 1 shows the first two combined EOFs for ERA5-NOAA, and the IFS-NEMO simulations for the 1979-2014 period. The first two principal components of ERA5-NOAA compare very well with the ones obtained in real-time by the Australian Bureau of Meteorology with a different set of observations for the 1979-2014 period, as supported by correlation of 0.93 and 0.97, respectively. Similar levels of agreement have been reported in previous analyses between different observation-based datasets (Rashid et al., 2011).

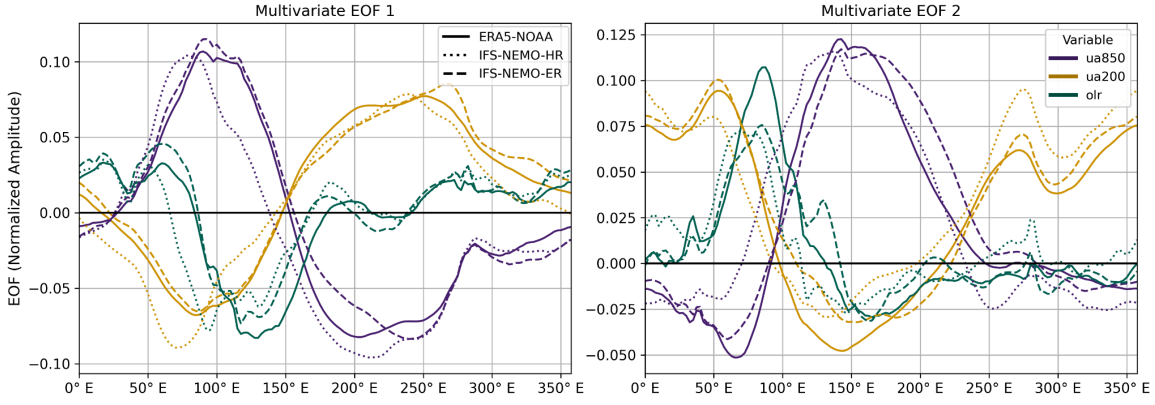

Figure 1: First two EOFs of the multivariate MJO dataset with ua850 (purple), ua200 (yellow) and OLR (green). Daily anomalies have been retrieved by removing the first three harmonics of the climatology and the previous 120 days mean. The continuous

https://doi.org/10.5194/egusphere-2026-3251
Preprint. Discussion started: 23 June 2026

lines show the EOFs of the ERA5-NOAA while dashed and dotted lines refer to IFS-NEMO-ER and -HR respectively. The EOFs have been swapped and their sign changed accordingly to match the WH04 order and structure.

The EOFs of the model have been switched and flipped when required to match the ERA5-NOAA structure for comparison purposes. While IFS-NEMO underestimates the relative and total amount of variance captured by the first two EOFs at both resolutions with respect to ERA5-NOAA (Table 1), with HR giving slightly better results, both show good agreement in terms of spatial distribution, as supported by the correlations in Table 2. IFS-NEMO-ER shows systematically better correlation values than IFS-NEMO-HR, in particular for OLR, which again supports a more realistic representation of the MJO spatial structure .

However, the lower correlation values for IFS-NEMO-HR may simply be a mathematical artifact arising from the strong degeneracy of the first two EOFs in that simulation (i.e., their explained variance is very similar), rather than an indication of deficiencies in the physical characterisation of the MJO. Indeed, previous works have highlighted how the physical interpretation of EOFs should be done carefully as not all the variance related to the MJO is captured by the first two EOFs (Roundy, 2015). We also see in Table 2 also that the relative contribution of each variable to the variance explained by the first 2 PCs as described by Ventrice et al. (2013), is very similar between both IFS-NEMO versions and also with ERA5-NOAA, with the models slightly overestimating the variance explained by the wind, and underestimating the variance explained by the OLR.

Dataset	Explained Variance EOF1+2 (%)	X_{ua850} (%)	X_{ua200} (%)	X_{OLR} (%)
ERA5-NOAA	13.4+13.1	46.0	38.5	15.5
IFS-NEMO-HR	10.2+9.3	48.5	39.7	11.8
IFS-NEMO-ER	10.7 +10.0	49.5	38.1	12.4

Table 1: (first column) variance explained by the first two EOFs in observations and IFS-NEMO. (columns 2-4) fractional contribution of each variable to the first two PCs with the methodology defined by Ventrice et al. (2013).

Model EOF	ua850	ua200	OLR
IFS-NEMO-HR EOF 1	0.95	0.95	0.82
IFS-NEMO-ER EOF 1	0.99	0.99	0.96
IFS-NEMO-HR EOF 2	0.91	0.94	0.82
IFS-NEMO-ER EOF 2	0.97	0.98	0.94

Table 2: spatial pattern correlation values of the first two EOFs of ERA5-NOAA and the corresponding EOFs of IFS-NEMO, computed over the 1979-2014 period.

https://doi.org/10.5194/egusphere-2026-3251
Preprint. Discussion started: 23 June 2026

We have also inspected the lag-correlation between the first two PCs of each dataset, which informs about the MJO propagation timescales as extracted by the EOF analysis. Figure 2 shows that the maximum correlation between the PCs takes place around day 9-10 for ERA5-NOAA and 1 day earlier in IFS-NEMO, at both resolutions. This may suggest a slightly faster phase progression in the model, which implies a faster eastward propagation, but the difference is small and falls within the uncertainty of the EOF-based lag-correlation approach, which is sensitive to sampling variability and the near-degeneracy of the leading MJO EOFs. The broader lag-correlation tail in IFS-NEMO may reflect weaker phase locking between the leading MJO modes, resulting in a wider and less regular range of effective propagation times.

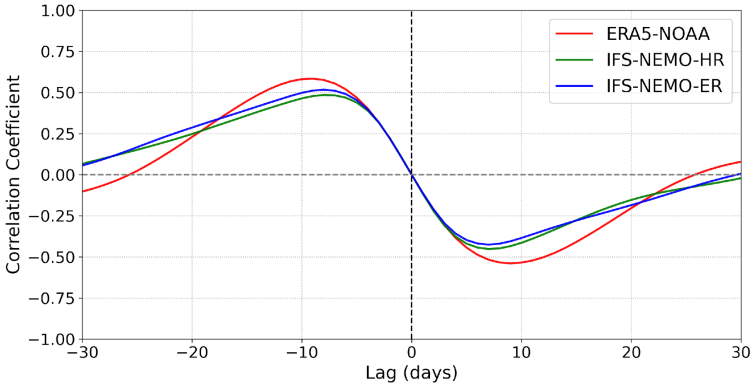

Figure 2: Lead-lag correlation between the first 2 PCs associated with the two leading EOFs of each dataset (i.e. ERA5-NOAA, IFS-NEMO-HR and ER). The sign and order of the PCs have been adjusted so that they are comparable across datasets.

An alternative approach to study MJO propagation, applied here following the methodology used in Kim et al. (2025), involves correlating meridionally averaged intraseasonal OLR and ua850 anomalies over a reference region over the Indian Ocean (defined as 75° E–100° E, 15° S–10° N) with the respective meridionally averaged anomalies at different longitudes and time lags, as illustrated in Fig. 3 for the 15° S–10° N band. This latitudinal range captures the core equatorial region where the MJO is most active, ensuring the analysis focuses on the dominant convective signal associated with its propagation.

https://doi.org/10.5194/egusphere-2026-3251
Preprint. Discussion started: 23 June 2026

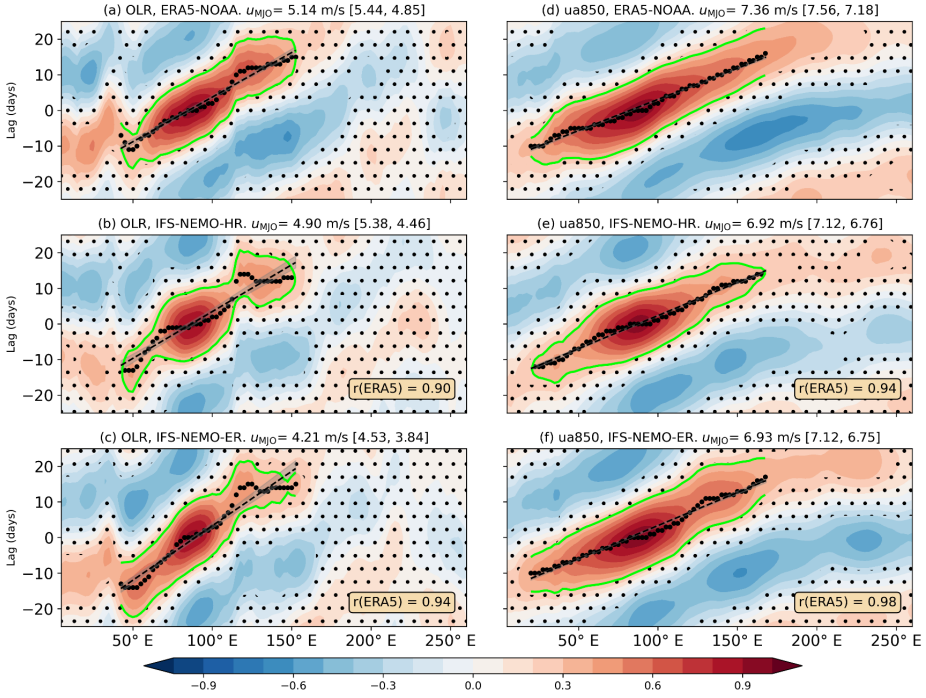

Figure 3: Lag - longitude maps of 15° S-10° N meridionally averaged OLR (a, b and c) and ua850 (d, e and f) anomalies correlation against the Indian Ocean region 75° E-100° E. The propagation speed has been computed following the approach of Kim et al. (2025). To ensure comparison between datasets the minimal common longitudinal range with significant correlation has been taken into account ([142.5° E-152° E] for OLR and [20° E-168° E] for ua850). The dashed line shows the linear fit, which has been computed only on 95% significance peaks. Significance has been adjusted accounting for autocorrelation with corrections following Zwiers and Von Storch (1995). The shaded grey band indicates the 95 % confidence level obtained from bootstrapping. Pattern correlations over the entire domain (5–260° E) between IFS-NEMO and ERA5 are shown in the yellow box.

Such correlation maps are computed for the 1979-2014 period for ERA5-NOAA for the boreal winter season (DJF). The propagation speed is obtained from the slope of a least-square linear regression and converted to m/s (see Data and methods). The best estimate of the propagation speed in the observational reference is 5.14 m s^{-1}, for IFS-NEMO-HR is 4.90 m s^{-1}, and for IFS-NEMO-ER is 4.21 m s^{-1}. Interestingly, the speed in IFS-NEMO-HR is consistent with ERA5 when considering the uncertainty described by the 95 % percentile range of a bootstrap, and also consistent with the speed in IFS-NEMO-ER. This analysis underscores the large uncertainties associated with estimating and comparing MJO propagation speeds. The pattern correlation score indicates that IFS-NEMO-ER better reproduces the correct signal propagation features. Both model versions struggle to reproduce the right eastward limit of the propagation and its extension beyond the Maritime Continent (i.e. beyond 150-160° E). This feature is commonly found in models when evaluating the eastward propagation of fields such as OLR. By contrast, this reduced eastward propagation is not present in the correlation map of ua850, especially for

https://doi.org/10.5194/egusphere-2026-3251
Preprint. Discussion started: 23 June 2026

IFS-NEMO-ER, which indicates that the underlying issue might be related to the timing of convection and not necessarily to the circulation dynamics. In fact, after deep convection is suppressed over the Western Pacific, the convective dynamics tend to decouple from the horizontal circulation and the propagation continues with a speed similar to that of Kelvin waves (Zhang, 2005). We finally note that the slope of the linear regression is sensitive to the choice of the correlation contour and the longitude range over which the regression is computed. However, this does not qualitatively affect the results.

Power spectra of the OLR anomalies have been also calculated to extract the variance of the simulated MJO from its temporal properties. Only the symmetric spectra is used in this analysis as it has been shown that the antisymmetric component does not retain significant power associated with the MJO (Wheeler and Kiladis, 1999; Dias et al., 2025). Figure 4 shows the significant power spectra and includes the well-known theoretical dispersion curves (in black) associated with equatorial Kelvin waves and Rossby waves (Ghil and Childress, 1987). For positive (negative) wavenumbers, significant peaks are associated with eastward (westward) propagating signals. The dashed lines between 1/30 days^{-1} and 1/80 days^{-1} for frequency and between 1 and 4 for wavenumber define the region in the wavenumber-frequency domain commonly linked to the MJO. Areas with significant peaks in both versions of IFS-NEMO generally coincide with the areas with significant peaks in observations. However, both model versions underestimate the spectral power of tropical waves and the MJO. Specifically, within the MJO domain (dashed box) the average power in IFS-NEMO is about 80 % of the observed one in both resolutions.

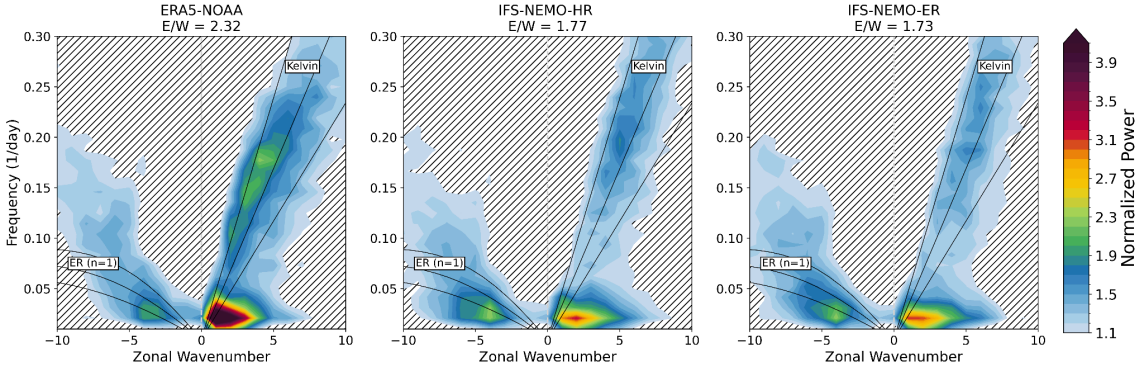

Figure 4: Wavenumber-frequency power spectrum of OLR as defined by Wheeler and Kiladis (1999). Significant power in the positive (negative) wavenumber domain refers to eastward (westward) propagating signals. Continuous black lines indicate theoretical dispersion curves for equatorial Rossby (negative wave numbers) and Kelvin (positive wave number) waves. The part of the domain associated with the MJO spans frequencies between 1/80 and 1/30 days^{-1} and wavenumbers between 1 and 4. The spectra have been normalised dividing by a red noise background spectrum. Hatched areas indicate regions with significance lower than 95 %.

This result is consistent with previous work by Chang et al. (2020) that did not detect any impact of horizontal resolution on this diagnostic, observing similar MJO power underestimation for two versions of CESM1.3 with nominal resolutions of 0.1° in the ocean (with 0.25° atmospheric resolution) and 1° in the ocean (with 1° atmospheric resolution). We note that both

https://doi.org/10.5194/egusphere-2026-3251
Preprint. Discussion started: 23 June 2026

IFS-NEMO versions overestimate the power of equatorial Rossby waves, and underestimate the power of Kelvin waves in the selected region. Figure 4 also shows the Eastward/Westward (E/W) ratios of power-weighted frequency between wavenumbers 1-4 and frequencies from 1/80 to 1/30 $days^{-1}$. The comparison of the E/W ratios indicates that IFS-NEMO underestimates the eastward propagation of organised convection.

We evaluate additional spatial aspects of the MJO looking at the composites of precipitation anomalies (Fig. 5) for each phase of the MJO. We first project the multivariate anomalies of each dataset onto the EOFs of ERA5-NOAA to ensure that phases are consistent for the three datasets. Latitudinally weighted pattern correlation has been computed to compare the composites in IFS-NEMO-HR and -ER with the observation-based dataset over the combined significant areas. Overall, IFS-NEMO-ER better captures the different patterns of ERA5, in particular for phases 4 and 5, while IFS-NEMO-HR only shows a higher correlation in phase 2. The model shows a more limited eastward propagation during the late phases, with much lower and locally confined positive anomalies in phases 7 and 8. This is the phase when the convective cluster has passed the Maritime Continent and is thus more exposed to the influence of sea surface temperatures over the equatorial Pacific. The deficient eastward propagation in later phases is therefore likely due to a combination of the Maritime Continent barrier known issue and a premature suppression of convection by the SST-convection feedback over the equatorial Pacific. Convection is sustained and driven eastward by warm SSTs developing ahead (east) of the MJO active center. The model's SST-convection feedback suppresses convection prematurely over the central/eastern Pacific, most likely due to the cold bias (see Section 3.2) in the Tropical Pacific Ocean, and prevents the correct eastward propagation of the MJO (H.-M. Kim et al., 2016).

https://doi.org/10.5194/egusphere-2026-3251
Preprint. Discussion started: 23 June 2026

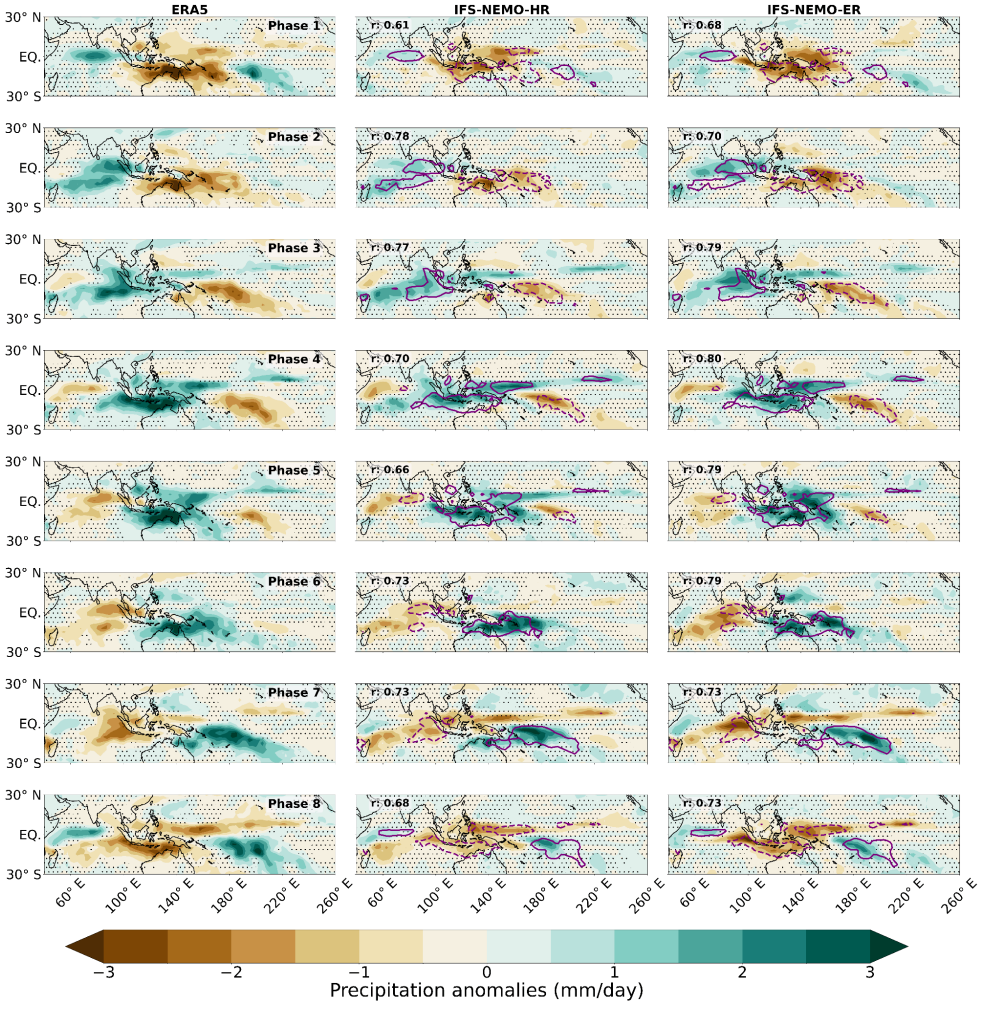

Figure 5: Anomaly composites of intraseasonal precipitation for (a) ERA5, (b) IFS-NEMO-HR and (c) IFS-NEMO-ER. The MJO phases are defined by the RMMs obtained projecting the multivariate anomalies of each dataset onto the EOFs of ERA5-OLR. Dotted areas mark statistically non-significant regions. Significance levels correspond to the 95 % confidence level from a bootstrapping distribution of n=1000 samples using all available DJF days. Weighted pattern correlation values shown in the top-left corner of each panel have been computed for the over the union of the significance masks between the two IFS-NEMO versions and ERA5. Purple contours are the reference ±2 mm day^{-1} contours from ERA5.

In order to explain the previous result, we additionally analysed composites of intraseasonal tropical specific humidity anomalies. The MJO can be framed within the moisture mode theory framework (Chang, 2020). In such theory the vertical and horizontal moisture gradients and advection drive the development of deep convection as well as the horizontal eastward propagation. Therefore, it is crucial for the model to correctly reproduce the humidity spatial distribution. The model correctly represents the main features seen in ERA5, with relatively high pattern correlation during all phases (Figure 6).

https://doi.org/10.5194/egusphere-2026-3251
Preprint. Discussion started: 23 June 2026

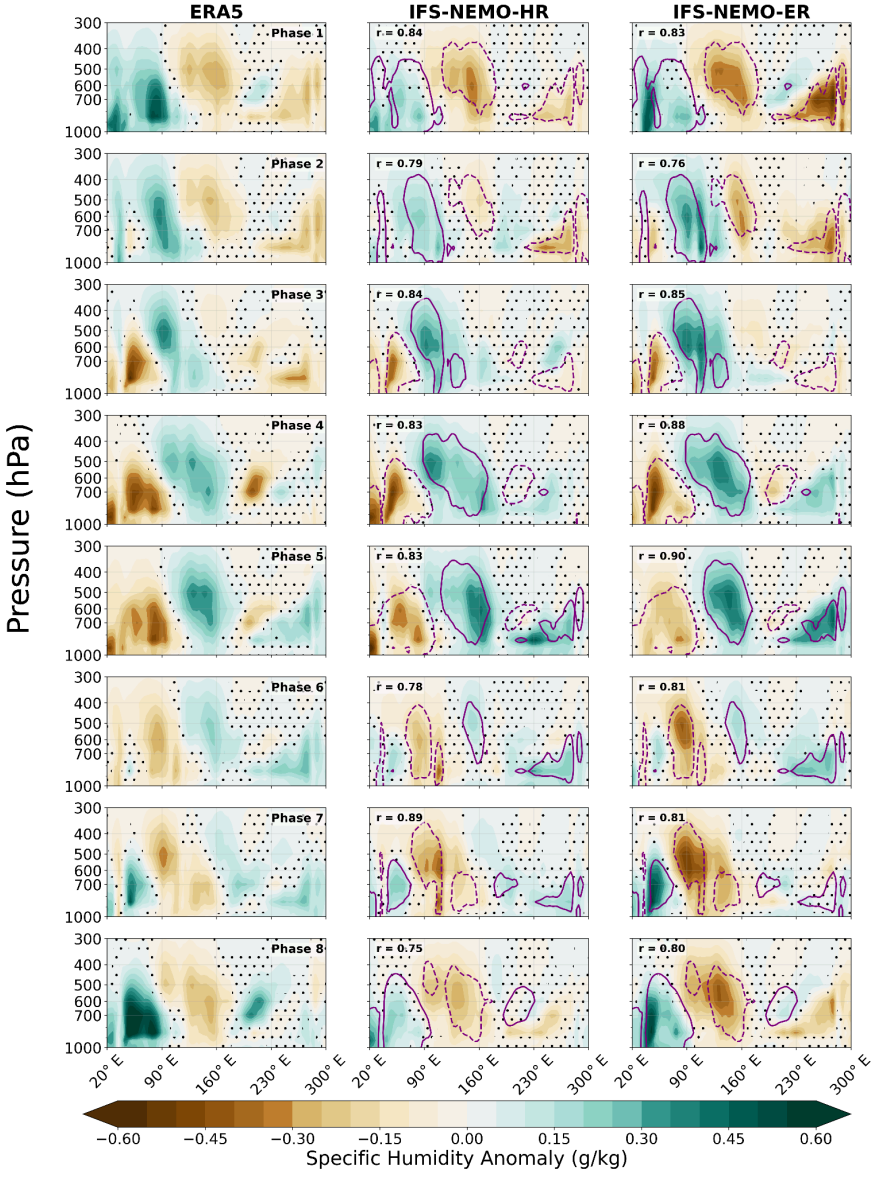

Figure 6: Anomalies composites of intraseasonal tropical (5º S-5º N) specific humidity vertical cross section for (a) ERA5, (b) IFS-NEMO-HR and (c) IFS-NEMO-ER. The MJO phases are defined by the RMMs obtained projecting the multivariate anomalies of each dataset onto the EOFs of the OBS. Dotted areas mark statistically non-significant regions. Significance levels have been computed at the 95 % level from a bootstrapping distribution of n=1000 samples from all available DJF days. Weighted pattern correlation values have been computed over the union of the significance masks between IFS-NEMO and ERA5. Purple contours are the reference ±0.15 g kg^{-1} contours from ERA5.

https://doi.org/10.5194/egusphere-2026-3251
Preprint. Discussion started: 23 June 2026

Increasing horizontal resolution in IFS-NEMO does not seem to improve the comparison with ERA5. Low-level moistening over the Indian Ocean warm pool is known to precede deep convection in the atmosphere at the beginning of an MJO cycle (D. Kim et al., 2009; Zhao et al., 2015). While such preconditioning is correctly located in both IFS-NEMO versions, its magnitude is underestimated (especially in phases 1 and 2) with a stronger dry bias in IFS-NEMO-HR. An early wet bias is found in proximity to the Maritime Continent in IFS-NEMO (phase 4). This condition does not favour the propagation of the MJO, as it could lead to anomalous descending atmospheric motion, preventing deep convection from happening (H.-R. Kim et al., 2016). Early strong positive anomalies are also found in IFS-NEMO over the Eastern-Pacific during phase 5. This indicates that moisture is not transported vertically efficiently enough in the model, and it is, on the other hand, propagated eastward relatively quickly, which explains the difficulties in sustaining convection past the Maritime Continent in IFS-NEMO. At the same time IFS-NEMO-ER tends to display drier conditions over the last phases of the MJO life cycle. The low level dry bias in both IFS-NEMO versions during the final phases of the MJO life cycle could be linked to the suppression of precipitation in the same phases over the Central Pacific (Fig. 5). Studies have suggested that increasing vertical resolution could actually improve the mid-troposphere clouds moistening and the vertical transport of water vapor and thus generate a more realistic deep convection generation (Zhang, 2005; Jiang et al., 2020). However, both IFS-NEMO versions use 137 levels in the vertical, which is considerably higher than the models surveyed in those studies, suggesting that vertical resolution alone is not the limiting factor and that the persistent deficiencies in deep convection generation are more likely rooted in the convective parameterization scheme itself.

3.2 Long term variability of the MJO

Understanding the multidecadal variability of the MJO is crucial for better anticipating its future changes. Several works have studied this long-term variability with reanalysis datasets to extend the analyses beyond the satellite era, combining different datasets (Oliver and Thompson, 2011; Cui and Li, 2022; Du et al., 2024; Dias et al., 2025; H.-R. Kim et al., 2025) and techniques (Dasgupta et al., 2020) to address both the MJO changes in activity and predictability. Although uncertainties remain, most of these studies have shown an increase of activity of the MJO over the historical period and have also investigated how the MJO is shaped by climate change and the physical mechanisms behind its response (Bui and Maloney, 2018, 2019; Lyu et al., 2019; Maloney et al., 2019; Bui et al., 2023). Understanding and evaluating the behaviour of the MJO over the past warming period is thus crucial to build trust on future projections of MJO activity.

This section focuses on the long term changes of MJO activity over the period 1950-2014 in ERA5 and the IFS-NEMO simulations. We first study how the MJO structure evolves along the study period by computing the MJO EOFs in 35 year rolling windows, replicating the methodology of Dias et al. (2025) but with longer time windows. We choose the 35-year window to match the same length covered by OLR satellite observations and because this comparatively longer window ensures smoother transitions when tracking the long-term variations in MJO activity, the frequency of the events and their spatial structure, by reducing the noise associated with other tropical waves and storms.

https://doi.org/10.5194/egusphere-2026-3251
Preprint. Discussion started: 23 June 2026

Figure 7 shows the two leading EOFs for ERA5, IFS-NEMO-HR and IFS-NEMO-ER for all the 35-year windows, allowing temporal overlap with a sliding step of one year. By looking at the spread of the EOFs we conclude that ERA5 has higher year to year variability in terms of MJO structure than both IFS-NEMO simulations. These year-to-year differences might be partly due to the sensitivity of the EOF results to the noise induced by Rossby and Equatorial Kelvin waves (Roundy et al. 2009).

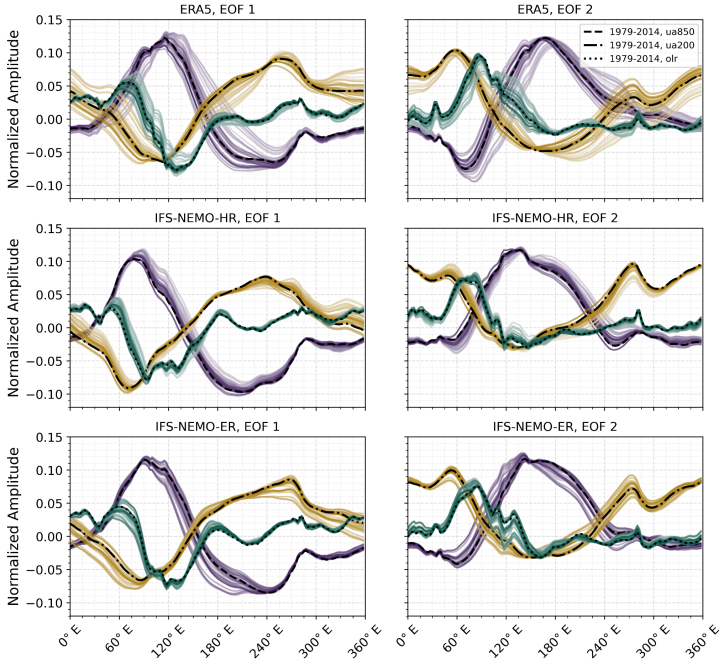

Figure 7: First two EOFs of the multivariate MJO dataset with ua850 (red), ua200 (green) and OLR (blue). for ERA5 and the IFS-NEMO simulations in each different 35 year rolling window. For each window, daily anomalies have been retrieved by removing the corresponding 35-year climatology and the previous 120 days mean. The EOFs have been swapped and their sign changed whenever needed to match WH04 order. Lighter shades correspond to earlier windows, while darker shades indicate later ones. The black line for each variable refers to the last 35 years.

Since the variability associated with the MJO is captured by the combination of two EOFs (Roundy, 2015), and given that their similar levels of explained variance make them prone to degeneracy (North et al., 1982), we use the total explained variance as a measure of the long term variability in MJO activity. The continuous lines in Figure 8a represent the variance as the sum of the eigenvalues associated with the first two modes of the EOF analysis per each window. The dashed lines represent the variance in the datasets reconstructed with the respective present-day EOFs. The dotted lines represent the variance in the dataset reconstructed by projecting onto the present-day ERA5-NOAA EOFs. As expected, the dashed lines converge towards the solid lines as for the last window the two methodologies are mathematically identical. Two shortcomings are exhibited by IFS-NEMO at both resolutions, which are evident for all the three different ways to project the variance explained backwards in time: the model underestimates the combined variance associated with the MJO and

https://doi.org/10.5194/egusphere-2026-3251
Preprint. Discussion started: 23 June 2026

fails to capture the long term upward trend found in ERA5. Such an increasing trend in MJO activity with rising ocean temperatures is consistent also with previous works based on both reanalysis datasets and simulations (Pohl and Matthews, 2007; Arnold et al., 2015; Dias et al., 2025). Indeed, regional SSTs are crucial to generate and sustain an active phase of the MJO (Jones and Carvalho, 2011; DeMott et al., 2014; H.-M. Kim et al., 2016).

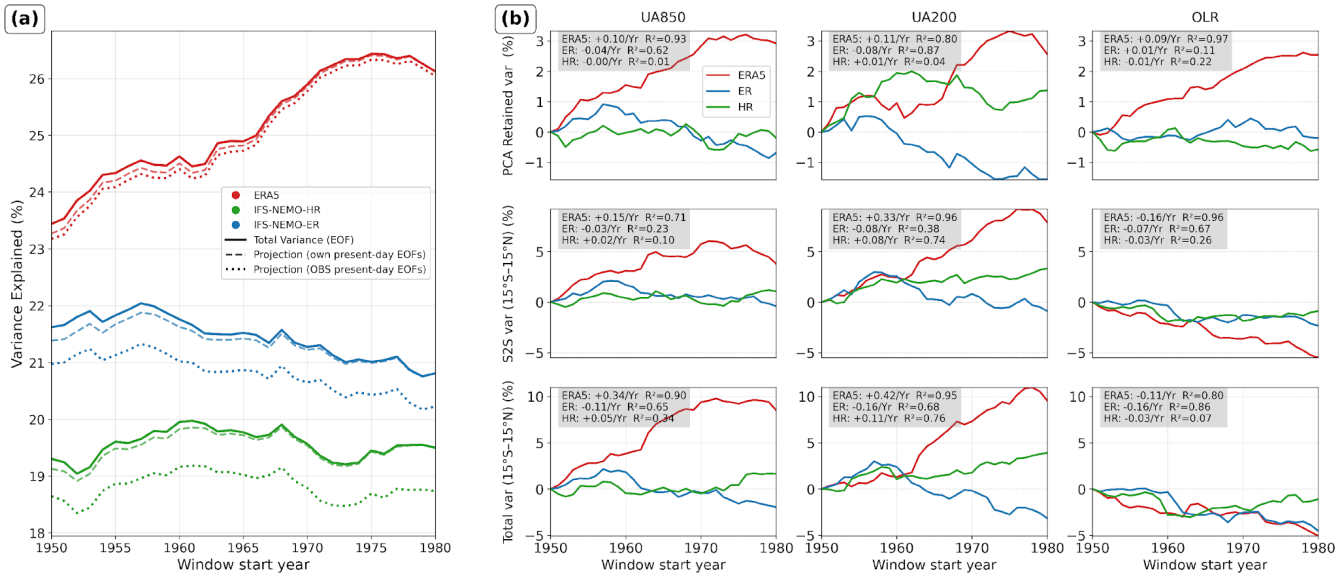

Figure 8: (a) MJO-related variance in each 35 year moving window as accounted for by the combined variance of the first two EOFs computed directly for each window (solid lines), reconstructed with the first two EOFs of the last window of the respective dataset (dashed lines) or reconstructed with the first two EOFs of the last window in ERA5-OLR (dotted lines). (b) Long-term changes in the variance of the three variables used in the multivariate EOF analysis of the MJO (i.e. UA850, UA200, OLR), computed in successive 35-year windows. Each row shows a different metric: (top) variance retained for each variable with the first two EOFs, (middle) variance of the intraseasonal tropical anomalies (15° S-15° N) used as input to the EOF analysis (filtered by removing the mean of the previous 120 days), and (bottom) total variance in the tropics. Red, green, and blue lines correspond to ERA5, IFS-NEMO-HR, and IFS-NEMO-ER, respectively. Linear trends and their R^2 values are indicated in the legend boxes.

To assess if the increase in MJO variance over the second half of the 20th century in reanalyses could be partly driven by the concomitant warming and expansion of the Indo-Pacific warm pool (IPWP) and the steady increase in atmospheric moisture with global warming, the MJO variance is compared to the long-term changes in IPWP. If the models underestimate SST trends in that region, or if the mean SST bias does not translate SST anomalies into enhanced deep convection efficiently enough, the MJO would not strengthen as observed. Also if the model convection scheme is not sensitive enough to column moisture, the simulations would fail to translate the moistening trend into stronger MJO variance. However, by inspecting the long term changes of the IPWP (Fig. 9a-b), we found a higher increase in total area in IFS-NEMO than in ERA5 while the changes in intensity are comparable. This indicates that the model IPWP temperatures correctly respond to the external

https://doi.org/10.5194/egusphere-2026-3251
Preprint. Discussion started: 23 June 2026

forcing and cannot therefore explain the misrepresentation of the evolution of the MJO variance. On the other hand, the reduced extent of the IPWP area compared to observations (an expression of a cold bias), shown in Fig. S3, could explain why the MJO variance is systematically underestimated in the model.

To further investigate why IFS-NEMO fails to simulate the increase in MJO activity over time, Fig. 8b assesses the long-term evolution of variance in each of the three variables entering the multivariate EOF analysis (i.e. UA850, UA200, and OLR) across successive 35-year windows according to three different levels of aggregation: the variance retained by the two leading EOFs, the variance of the intraseasonal anomalies directly used for the EOF analysis and the total variance of each variable in the Tropics (15° S-15° N).

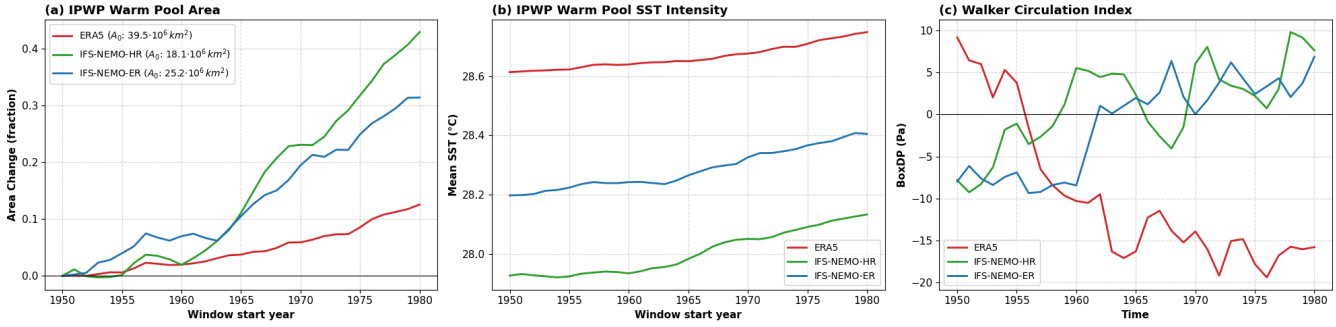

Figure 9: Time series of: 35-year averages of Indo-Pacific Warm Pool extension anomaly with respect to the period 1950-1984 (a) and intensity (b). The IPWP area is defined as the region where the climatological sea surface temperatures exceed the 28 °C threshold. The intensity anomaly is computed for each window as the area-weighted average over the warm pool region of ERA5. Time series of the WC strength (c) averaged over 35-year windows for ERA5, IFS-NEMO-HR and IFS-NEMO-ER. The recent observed strengthening of the WC is not visible because of the length of the smoothing window.

The most remarkable feature in ERA5 is a strong increasing trend in the variance of the low and high troposphere zonal winds, already reported in Maloney et al. (2019), which is consistent for all temporal aggregations. By contrast, IFS-NEMO simulations show near-zero or slightly negative trends for all variables and metrics. Interestingly for OLR, while ERA5 shows a robust decrease in its total and intraseasonal variance, also exhibited by the models, its MJO-related variance substantially increases over time, with the models showing a largely stable evolution. The decrease in total and intraseasonal OLR variance alongside the increase in MJO-related OLR variance in ERA5 suggests that the MJO is becoming an increasingly efficient organizer of tropical convection over time, concentrating a growing fraction of convective activity into coherent intraseasonal events; the failure of the models to reproduce this shift, despite capturing the overall decrease in OLR variance, points to a specific deficiency in the representation of MJO convective organization rather than in the simulation of the background convective environment. We highlight that, as indicated by the results of Table 1, the horizontal atmospheric circulation plays a major role in characterising the EOFs as defined by WH04, with OLR only contributing around 15 % in observations and less than 12 % in IFS-NEMO, a proportion that stays constant throughout the full period (not shown here).

https://doi.org/10.5194/egusphere-2026-3251
Preprint. Discussion started: 23 June 2026

Figure 8b suggests that the long term changes in the background atmospheric circulation are misrepresented in IFS-NEMO. Specifically, the MJO is directly intertwined with the WC as the main center of convective dynamics of the MJO moves across the Maritime Continent and develops right to the west of the upward branch of the Walker cell (Chen and Wang, 2018). Previous works have studied the impact of the WC strength on the MJO propagation speed (Suematsu and Miura, 2022) and have highlighted the impacts of WC bias on the correct evolution of the MJO (H.-M. Kim et al., 2016, Suematsu et al., 2022).

We compared the time series of the WC intensity over time between ERA5 and IFS-NEMO (Fig. 9c). We found that ERA5 reproduces the well known weakening of the WC observed over the second half of the 20th Century. The recent observed strengthening of WC intensity (Power et al., 2021) appears as merely a slow-down of the weakening trend in the plot for ERA5, since the positive trend is smoothed out by the 35-year running mean. On the other hand, IFS-NEMO shows quite the opposite trends and with weaker amplitude. We note that there is no consensus on whether the recent changes in the WC are due to internal tropical decadal variability or the result of human-induced external forcing (Chung et al., 2019; Power et al., 2021). By inspecting all possible 35-year long windows in IFS-NEMO (following the methods of Kociuba and Power, 2015) we did not detect any significant trend (in either direction), indicating that the model memory is much shorter with respect to ERA5, which prevents it from developing the right kind of internal variability either.

These WC shortcomings in IFS-NEMO-HR and IFS-NEMO-ER explain why the models fail to capture the long term trend of the variance retained for each variable and for the total variance associated with the MJO. Specifically, an increase in the WC strength manifests as a positive easterly anomaly over the Maritime Continent, where the ascending branch of the WC is located. This would result in dry air advection into the western Pacific (H.-M. Kim et al., 2016), hindering the correct development of the MJO.

We also investigated the changes in activity observed for each of the eight different MJO phases, as the long term response to the global warming forcing does not take place homogeneously over the entire tropical basin explored during a full MJO cycle. Figure 10 shows the number of active days per phase and the mean MJO amplitude during those days when the MJO is computed by projecting the anomalies of each 35-year window onto ERA5-NOAA present-day EOFs.

https://doi.org/10.5194/egusphere-2026-3251
Preprint. Discussion started: 23 June 2026

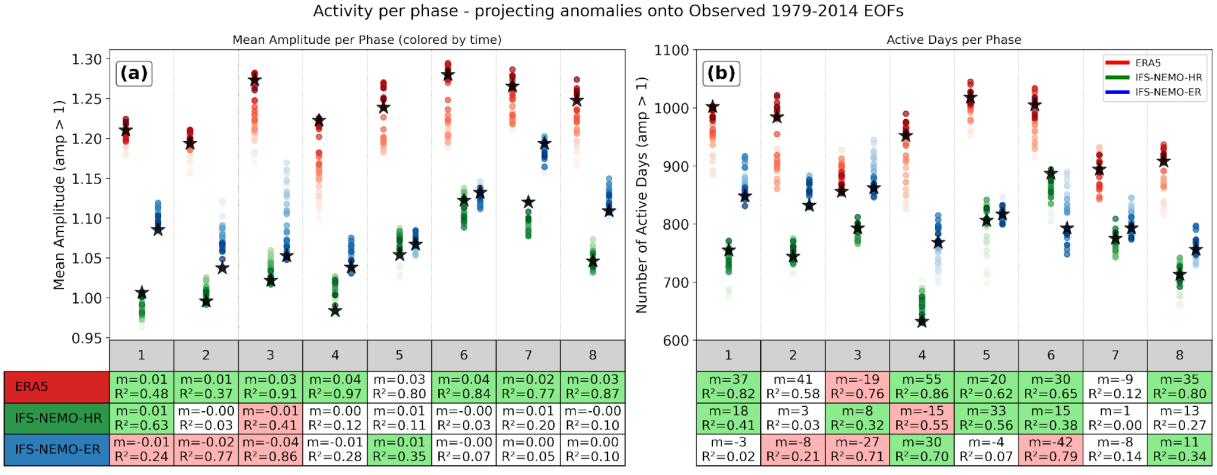

	1	2	3	4	5	6	7	8
ERA5	m=0.01 R²=0.48	m=0.01 R²=0.37	m=0.03 R²=0.91	m=0.04 R²=0.97	m=0.03 R²=0.80	m=0.04 R²=0.84	m=0.02 R²=0.77	m=0.03 R²=0.87
IFS-NEMO-HR	m=0.01 R²=0.63	m=-0.00 R²=0.03	m=-0.01 R²=0.41	m=0.00 R²=0.12	m=0.01 R²=0.11	m=-0.00 R²=0.03	m=0.01 R²=0.20	m=-0.00 R²=0.10
IFS-NEMO-ER	m=-0.01 R²=0.24	m=-0.02 R²=0.77	m=-0.04 R²=0.86	m=-0.01 R²=0.28	m=0.01 R²=0.35	m=-0.00 R²=0.07	m=0.00 R²=0.05	m=0.00 R²=0.10

	1	2	3	4	5	6	7	8
ERA5	m=37 R²=0.82	m=41 R²=0.58	m=-19 R²=0.76	m=55 R²=0.86	m=20 R²=0.62	m=30 R²=0.65	m=-9 R²=0.12	m=35 R²=0.80
IFS-NEMO-HR	m=18 R²=0.41	m=3 R²=0.03	m=8 R²=0.32	m=-15 R²=0.55	m=33 R²=0.56	m=15 R²=0.38	m=1 R²=0.00	m=13 R²=0.27
IFS-NEMO-ER	m=-3 R²=0.02	m=-8 R²=0.21	m=-27 R²=0.71	m=30 R²=0.70	m=-4 R²=0.07	m=-42 R²=0.79	m=-8 R²=0.14	m=11 R²=0.34

Figure: 10: Evolution of the mean amplitude (left) and number of active days (right) per MJO phase in ERA5 and the IFS-NEMO simulations for each 35-year year window (going from light to darker shades as time progresses). Only the active days for each phase are considered. In all datasets, the phases have been defined projecting the multivariate anomalies on the EOFs for the last 35-year window of ERA5. Black stars mark the value for the last 35-year window. The table shows the slope per decade of the trend of the MJO mean amplitude and number of active days, together with the R^2 value of the linear fit. In the table, green (red) cells indicate a significantly positive (negative) trend in the respective metric, while non-significant trends are not highlighted.

In ERA5 all phases display an increase in the mean amplitude, with strongest changes found over phases 4 to 6, which correspond to the passing of the main convective center of the MJO over the regions of the IPWP (Yoo et al., 2011). A significant but weaker increase is also found in phases 7 and 8, with less clear trends for the first two phases.

None of the IFS-NEMO simulations consistently captures the observed increase in MJO amplitude in most phases. We also note that both model versions, and especially IFS-NEMO-HR, systematically underestimate the activity of the MJO when phases are defined using the present-day ERA5-OLR EOFs; however, this is likely an artifact of the projection, as activity becomes comparable for all phases between ERA5 and IFS-NEMO when each dataset is projected onto its own present-day EOFs (Fig. S4). This suggests that the MJO, on average, is as active in IFS-NEMO as it is in ERA5, but with a spatially and temporally different structure. In terms of active days per phase, ERA5 shows an increase over time for all phases but the third one, which shows a clear decrease. This suggests that the MJO is spending more time in all basins except on the western side of the Maritime Continent, possibly reflecting a change in propagation characteristics through all regions. None of the simulations reproduce these phase-dependent changes in activity.

The previous results highlight a different modulation by global warming of the MJO and its spatiotemporal characteristics in ERA5 and both IFS-NEMO configurations. Such a discrepancy is relevant due to its implications for MJO predictability.

Figure 11 shows the changes in weighted permutation entropy for the RMM amplitude, as defined in Du et al. (2024).

https://doi.org/10.5194/egusphere-2026-3251
Preprint. Discussion started: 23 June 2026

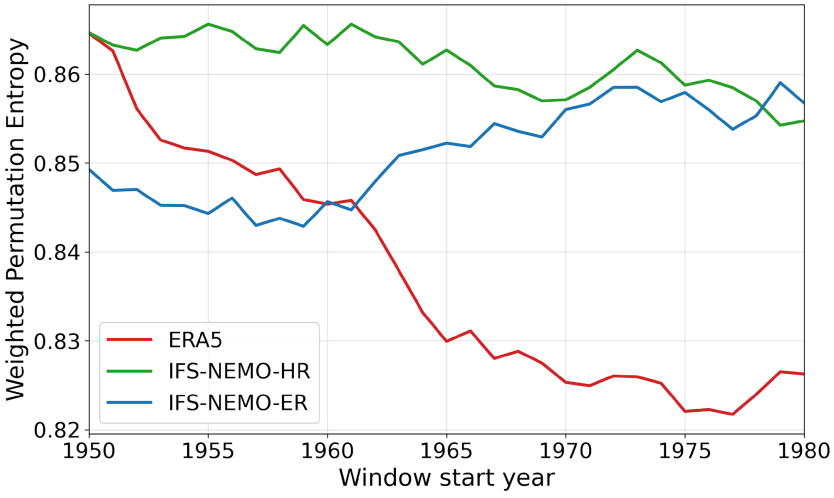

Figure 11: Time series of the WPE for the MJO amplitude over 35-year moving windows computed following the methodology described by Du et al. (2024) with the embedding parameter m=5 and the time delay τ=3. Similar results can be obtained using different parameters, which do not affect the conclusions. The WPE can be interpreted as a measure of the predictability of the time series, where a negative (positive) trend indicates an increase (decrease) in predictability.

For clarity and in the light of the results of Fig. 7b, we show the changes in WPE only for the case that RMMs are computed by projecting the multivariate anomalies of each dataset onto the respective present-day EOFs. The weakening trend in WPE for ERA5, indicative of an increase in predictability, is consistent with the results of Du et al. (2024), with the difference that interannual variability is smoothed out in our analysis because of the larger window length. Interestingly, the trend of WPE in both IFS-NEMO runs does not follow the expected behaviour and remains roughly flat, which suggests that the model is unable to represent — and leverage — the externally forced predictive component of the MJO.

4. Conclusions and final remarks

This study evaluates the MJO representation and long-term variability in two historical HighResMIP simulations with IFS-NEMO, a coupled atmosphere-ocean GCM. One of the simulations was run at standard ocean resolution (HR, ~25 km) and another with an eddy-resolving ocean (ER, ~9 km), with atmospheres that match the ocean resolution in both configurations. The eddy-resolving version has the potential of improving the representation of the MJO by better resolving the ocean-atmospheric coupling as well as the Maritime Continent topography. The evaluation reveals a nuanced picture of the impact of the resolution: the ER configuration brings some improvements in the representation of the fundamental spatio-temporal characteristics of the present-day MJO, which are very well captured by IFS-NEMO-HR and IFS-NEMO-ER. Specifically, increasing the model's horizontal resolution improves the spatial structure of the two leading EOFs of the multivariate intraseasonal anomalies dataset, as well as the EOFs variance explained suggesting the overall MJO activity is better constrained at higher resolution. Furthermore, IFS-NEMO-ER correctly reproduces the spatial features of

https://doi.org/10.5194/egusphere-2026-3251
Preprint. Discussion started: 23 June 2026

the leading EOFs, with higher OLR pattern correlations than IFS-NEMO-HR, suggesting improved coupling between deep convection and horizontal circulation.

However, both versions show lower explained variance than the observed MJO, which is also reflected in an underestimation of the wavenumber–frequency spectral peaks associated with the MJO. The horizontal resolution does not consistently improve the signal propagation of the MJO-related intraseasonal ua850 and OLR anomalies either. Indeed, the propagation speed is better in IFS-NEMO-HR than IFS-NEMO-ER when compared to observations or ERA5. However, IFS-NEMO-ER extends the eastward reach of the MJO's zonal wind signal compared to IFS-NEMO-HR, with the ua850 correlation map showing a more realistic propagation further into the western Pacific, although similar improvements are not seen for convective fields such as OLR or precipitation. Furthermore, IFS-NEMO does not correctly propagate the convective signal across the Maritime Continent at both resolutions, pointing to deficiencies that are not limited by grid spacing alone. In fact, if we interpret it as a moisture mode, the MJO depends on a strong low-level humidity gradient to sustain and propagate its convective envelope eastward. The dry bias present in IFS-NEMO during phase 1, when the main convective centre is located over the Indian Ocean, weakens this gradient in the Indo-Pacific region, reducing the moisture advection that would otherwise support propagation into and beyond the Maritime Continent. An excessive moisture injection in IFS-NEMO takes place during phases 3, 4 and 5. Such a late moisture accumulation results in a stronger positive anomaly over the Eastern Pacific rather than in the observed deep convection and cloud formation areas, which further suppresses the signal in later phases. Importantly, this bias is not alleviated by increasing horizontal resolution, and vertical resolution is unlikely to be the limiting factor either, as both IFS-NEMO configurations already use 137 levels, considerably more than models in which vertical resolution has been identified as a constraint. The evidence therefore points to the convective parameterization scheme itself as the primary source of this persistent bias.

Beyond present-day biases, the failure to reproduce the long-term increase in MJO activity raises more fundamental concerns for climate projections and initialized predictions. Neither IFS-NEMO configuration reproduces the observed positive trend in MJO-related variance seen in ERA5, a key limitation likely linked to a misrepresentation of the atmospheric circulation response to the external forcing. ERA5 captures the well-known weakening of the Walker Circulation over the second half of the 20th century, as well as its more recent strengthening, both of which are closely tied to the modulation of MJO activity through changes in the background tropical circulation. IFS-NEMO, by contrast, exhibits the opposite Walker Circulation trend with much weaker amplitude, and no significant trend is detected across any of the 35-year windows explored, suggesting that the model's memory is too short to develop the right kind of internal variability, failing also to capture the externally forced changes in tropical circulation. By contrast, the background ocean conditions in IFS-NEMO correctly respond to the external forcing, although the model's IPWP relatively increases in size and intensity more than in ERA5. Such a positive trend is not leading the trend in MJO variance in the case of IFS-NEMO. The model exhibits a cold ocean bias that is less prominent in the ER configuration, which could explain why IFS-NEMO-ER lowers the bias in total variance of the leading EOFs. However, we note that the cold tropical SST bias in IFS-NEMO complicates the interpretation of the long-term trend results, as this mean state error may dominate over, and partially mask, the model response to the external

https://doi.org/10.5194/egusphere-2026-3251
Preprint. Discussion started: 23 June 2026

forcing. Addressing these uncertainties through multi-model comparisons and better constraints on tropical mean state biases will be essential for building confidence in model-based projections of future MJO behaviour.

The misrepresentation of the background atmospheric state affects directly the MJO in IFS-NEMO, as the model fails to capture the positive trend in MJO-related variance seen in ERA5. The weighted permutation entropy of the RMMs remains flat in both configurations, indicating that IFS-NEMO cannot leverage the growing predictable component of the MJO that observations suggest is emerging under climate change.

Code and data availability

ERA5: Fifth generation of ECMWF atmospheric reanalyses of the global climate. Copernicus Climate Change Service Climate Data Store (CDS). https://cds.climate.copernicus.eu/#!/search?text=ERA5&type=dataset .

NOAA Interpolated Outgoing Longwave Radiation (OLR) data are provided by the NOAA PSL, Boulder, Colorado, USA, from their website at https://psl.noaa.gov .

IFS-NEMO simulations: *in the process of being published in the ESGF portal.*

The code used to produce the figures will be available in the final version. It is already available upon request to the corresponding author. We used the implementation of the algorithm of Wheeler and Kiladis (1999) from the library https://github.com/brianpm/wavenumber_frequency

Supplement link

The link to the supplement will be included by Copernicus, if applicable.

Author contributions

BM, PO and FD contributed to conceptualization; BM contributed to formal analysis; PO and FD contributed to project administration; NR, MA and DK contributed to data curation; BM and PO contributed to writing – original draft; BM, PO and FD contributed to writing – review & editing. All authors read and approved the final manuscript.

Competing interests

The authors declare that they have no conflict of interest.

https://doi.org/10.5194/egusphere-2026-3251
Preprint. Discussion started: 23 June 2026

Disclaimer

Views and opinions expressed are those of the author(s) only and do not necessarily reflect those of the European Union or the European Commission. Neither the European Union nor the European Commission can be held responsible for them.

Acknowledgements

It is a pleasure to acknowledge Alba Santos Espeso, Bianca Mezzina, Eneko Martin Martinez and Vincent Verjans for the insightful exchanges and feedback on the analysis carried out. We would also like to thank the BSC colleagues of the Climate Variability and Change for the productive discussion and the technical support.

Financial support

The work presented in this paper has been produced in the context of the European Union's Destination Earth Initiative and relates to tasks entrusted by the European Union to the European Centre for Medium-Range Weather Forecasts implementing part of this Initiative with funding by the European Union.
The research leading to these results has received funding from the EU HE Framework Programme under GA 101081383.
Some of the authors have received support of the GLORIA project (TED2021-129543B-I00) funded by the Spanish MICIN/AEI.

Review statement

The review statement will be added by Copernicus Publications listing the handling editor as well as all contributing referees according to their status anonymous or identified.

References

Afyouni, S., Smith, S. M., and Nichols, T. E.: Effective degrees of freedom of the Pearson's correlation coefficient under autocorrelation, NeuroImage, 199, 609–625, https://doi.org/10.1016/j.neuroimage.2019.05.011, 2019.

Ahn, M., Kim, D., Kang, D., Lee, J., Sperber, K. R., Gleckler, P. J., Jiang, X., Ham, Y., and Kim, H.: MJO Propagation Across the Maritime Continent: Are CMIP6 Models Better Than CMIP5 Models?, Geophys. Res. Lett., 47, e2020GL087250, https://doi.org/10.1029/2020GL087250, 2020.

https://doi.org/10.5194/egusphere-2026-3251
Preprint. Discussion started: 23 June 2026

Arnold, N. P., Branson, M., Kuang, Z., Randall, D. A., and Tziperman, E.: MJO Intensification with Warming in the Superparameterized CESM, J. Clim., 28, 2706–2724, https://doi.org/10.1175/JCLI-D-14-00494.1, 2015.

Bandt, C. and Pompe, B.: Permutation Entropy: A Natural Complexity Measure for Time Series, Phys. Rev. Lett., 88, 174102, https://doi.org/10.1103/PhysRevLett.88.174102, 2002.

Bui, H. X. and Maloney, E. D.: Changes in Madden-Julian Oscillation Precipitation and Wind Variance Under Global Warming, Geophys. Res. Lett., 45, 7148–7155, https://doi.org/10.1029/2018GL078504, 2018.

Bui, H. X. and Maloney, E. D.: Mechanisms for Global Warming Impacts on Madden–Julian Oscillation Precipitation Amplitude, J. Clim., 32, 6961–6975, https://doi.org/10.1175/JCLI-D-19-0051.1, 2019.

Bui, H. X., Li, Y.-X., Maloney, E. D., Kim, J.-E., Lee, S.-S., and Yu, J.-Y.: Emergence of Madden-Julian oscillation precipitation and wind amplitude changes in a warming climate, Npj Clim. Atmospheric Sci., 6, 22, https://doi.org/10.1038/s41612-023-00344-z, 2023.

Cao, C., Zhong, X., Chen, L., Wua, Z., and Li, H.: Enhanced predictions of the Madden-Julian oscillation using the FuXi-S2S machine learning model: Insights into physical mechanisms, https://doi.org/10.48550/ARXIV.2508.16041, 2025.

Chang, P., Zhang, S., Danabasoglu, G., Yeager, S. G., Fu, H., Wang, H., Castruccio, F. S., Chen, Y., Edwards, J., Fu, D., Jia, Y., Laurindo, L. C., Liu, X., Rosenbloom, N., Small, R. J., Xu, G., Zeng, Y., Zhang, Q., Bacmeister, J., Bailey, D. A., Duan, X., DuVivier, A. K., Li, D., Li, Y., Neale, R., Stössel, A., Wang, L., Zhuang, Y., Baker, A., Bates, S., Dennis, J., Diao, X., Gan, B., Gopal, A., Jia, D., Jing, Z., Ma, X., Saravanan, R., Strand, W. G., Tao, J., Yang, H., Wang, X., Wei, Z., and Wu, L.: An Unprecedented Set of High-Resolution Earth System Simulations for Understanding Multiscale Interactions in Climate Variability and Change, J. Adv. Model. Earth Syst., 12, e2020MS002298, https://doi.org/10.1029/2020MS002298, 2020.

Chen, G. and Wang, B.: Effects of Enhanced Front Walker Cell on the Eastward Propagation of the MJO, J. Clim., 31, 7719–7738, https://doi.org/10.1175/JCLI-D-17-0383.1, 2018.

Chung, E.-S., Timmermann, A., Soden, B. J., Ha, K.-J., Shi, L., and John, V. O.: Reconciling opposing Walker circulation trends in observations and model projections, Nat. Clim. Change, 9, 405–412, https://doi.org/10.1038/s41558-019-0446-4, 2019.

https://doi.org/10.5194/egusphere-2026-3251
Preprint. Discussion started: 23 June 2026

Cui, J. and Li, T.: Changes in MJO Characteristics and Impacts in the Past Century, J. Clim., 35, 577–590, https://doi.org/10.1175/JCLI-D-21-0306.1, 2022.

Dasgupta, P., Metya, A., Naidu, C. V., Singh, M., and Roxy, M. K.: Exploring the long-term changes in the Madden Julian Oscillation using machine learning, Sci. Rep., 10, 18567, https://doi.org/10.1038/s41598-020-75508-5, 2020.

DeMott, C. A., Klingaman, N. P., and Woolnough, S. J.: Atmosphere-ocean coupled processes in the Madden-Julian oscillation, Rev. Geophys., 53, 1099–1154, https://doi.org/10.1002/2014RG000478, 2015.

Dias, J., Gehne, M., Kiladis, G. N., Wolding, B., and Hoell, A.: Robust Multi-Decadal Variability of Madden-Julian Oscillation Amplitude in the 20th Century, Geophys. Res. Lett., 52, e2024GL113303, https://doi.org/10.1029/2024GL113303, 2025.

Doblas-Reyes, F. J., Kontkanen, J., Sandu, I., Acosta, M., Al Turjmam, M. H., Alsina-Ferrer, I., Andrés-Martínez, M., Arriola, L., Axness, M., Batlle Martín, M., Bauer, P., Becker, T., Beltrán, D., Beyer, S., Bockelmann, H., Bretonnière, P.-A., Cabaniols, S., Caprioli, S., Castrillo, M., Chandrasekar, A., Cheedela, S., Correal, V., Danovaro, E., Davini, P., Enkovaara, J., Frauen, C., Früh, B., Gaya Àvila, A., Ghinassi, P., Ghosh, R., Ghosh, S., González, I., Grayson, K., Griffith, M., Hadade, I., Haine, C., Hartick, C., Haus, U.-U., Hearne, S., Järvinen, H., Jiménez, B., John, A., Juchem, M., Jung, T., Kegel, J., Kelbling, M., Keller, K., Kinoshita, B., Kiszler, T., Klocke, D., Kluft, L., Koldunov, N., Kölling, T., Kolstela, J., Kornblueh, L., Kosukhin, S., Lacima-Nadolnik, A., Leal Rojas, J. J., Lehtiranta, J., Lunttila, T., Luoma, A., Manninen, P., Medvedev, A., Milinski, S., Mohammed, A. O. A., Müller, S., Naryanappa, D., Nazarova, N., Niemelä, S., Niraula, B., Nortamo, H., Nummelin, A., Nurisso, M., Ortega, P., Paronuzzi, S., Pedruzo Bagazgoitia, X., Pelletier, C., Peña, C., Polade, S., Pradhan, H., Quintanilla, R., Quintino, T., Rackow, T., Räisänen, J., Rajput, M. M., Redler, R., Reuter, B., Rocha Monteiro, N., Roura-Adserias, F., Ruppert, S., Sayed, S., Schnur, R., Sharma, T., Sidorenko, D., Sievi-Korte, O., Soret, A., Steger, C., Stevens, B., Streffing, J., et al.: The Destination Earth digital twin for climate change adaptation, https://doi.org/10.5194/egusphere-2025-2198, 13 August 2025.

Du, D., Subramanian, A. C., Han, W., Chapman, W. E., Weiss, J. B., and Bradley, E.: Increase in MJO predictability under global warming, Nat. Clim. Change, 14, 68–74, https://doi.org/10.1038/s41558-023-01885-0, 2024.

Fowler, M. D. and Pritchard, M. S.: Regional MJO Modulation of Northwest Pacific Tropical Cyclones Driven by Multiple Transient Controls, Geophys. Res. Lett., 47, e2020GL087148, https://doi.org/10.1029/2020GL087148, 2020.

https://doi.org/10.5194/egusphere-2026-3251
Preprint. Discussion started: 23 June 2026

Ghil, M. and Childress, S.: Topics in Geophysical Fluid Dynamics: Atmospheric Dynamics, Dynamo Theory, and Climate Dynamics, Springer New York, New York, NY, https://doi.org/10.1007/978-1-4612-1052-8, 1987.

Gottschalck, J., Wheeler, M., Weickmann, K., Vitart, F., Savage, N., Lin, H., Hendon, H., Waliser, D., Sperber, K., Nakagawa, M., Prestrelo, C., Flatau, M., and Higgins, W.: A Framework for Assessing Operational Madden–Julian Oscillation Forecasts: A CLIVAR MJO Working Group Project, Bull. Am. Meteorol. Soc., 91, 1247–1258, https://doi.org/10.1175/2010BAMS2816.1, 2010.

Gurvan, M., Bourdallé-Badie, R., Chanut, J., Clementi, E., Coward, A., Ethé, C., Iovino, D., Lea, D., Lévy, C., Lovato, T., Martin, N., Masson, S., Mocavero, S., Rousset, C., Storkey, D., Vancoppenolle, M., Müeller, S., Nurser, G., Bell, M., and Samson, G.: NEMO ocean engine, https://doi.org/10.5281/ZENODO.3878122, 2019.

Haarsma, R. J., Roberts, M. J., Vidale, P. L., Senior, C. A., Bellucci, A., Bao, Q., Chang, P., Corti, S., Fučkar, N. S., Guemas, V., Von Hardenberg, J., Hazeleger, W., Kodama, C., Koenigk, T., Leung, L. R., Lu, J., Luo, J.-J., Mao, J., Mizielinski, M. S., Mizuta, R., Nobre, P., Satoh, M., Scoccimarro, E., Semmler, T., Small, J., and Von Storch, J.-S.: High Resolution Model Intercomparison Project (HighResMIP v1.0) for CMIP6, Geosci. Model Dev., 9, 4185–4208, https://doi.org/10.5194/gmd-9-4185-2016, 2016.

Hersbach, H., Bell, B., Berrisford, P., Hirahara, S., Horányi, A., Muñoz-Sabater, J., Nicolas, J., Peubey, C., Radu, R., Schepers, D., Simmons, A., Soci, C., Abdalla, S., Abellan, X., Balsamo, G., Bechtold, P., Biavati, G., Bidlot, J., Bonavita, M., De Chiara, G., Dahlgren, P., Dee, D., Diamantakis, M., Dragani, R., Flemming, J., Forbes, R., Fuentes, M., Geer, A., Haimberger, L., Healy, S., Hogan, R. J., Hólm, E., Janisková, M., Keeley, S., Laloyaux, P., Lopez, P., Lupu, C., Radnoti, G., De Rosnay, P., Rozum, I., Vamborg, F., Villaume, S., and Thépaut, J.: The ERA5 global reanalysis, Q. J. R. Meteorol. Soc., 146, 1999–2049, https://doi.org/10.1002/qj.3803, 2020.

Holloway, C. E., Woolnough, S. J., and Lister, G. M. S.: The Effects of Explicit versus Parameterized Convection on the MJO in a Large-Domain High-Resolution Tropical Case Study. Part I: Characterization of Large-Scale Organization and Propagation*, J. Atmospheric Sci., 70, 1342–1369, https://doi.org/10.1175/JAS-D-12-0227.1, 2013.

Jiang, X., Su, H., and Waliser, D. E.: A Damping Effect of the Maritime Continent for the Madden-Julian Oscillation, J. Geophys. Res. Atmospheres, 124, 13693–13713, https://doi.org/10.1029/2019JD031503, 2019.

https://doi.org/10.5194/egusphere-2026-3251
Preprint. Discussion started: 23 June 2026

Jiang, X., Adames, Á. F., Kim, D., Maloney, E. D., Lin, H., Kim, H., Zhang, C., DeMott, C. A., and Klingaman, N. P.: Fifty Years of Research on the Madden-Julian Oscillation: Recent Progress, Challenges, and Perspectives, J. Geophys. Res. Atmospheres, 125, e2019JD030911, https://doi.org/10.1029/2019JD030911, 2020.

Kessler, W. S. and Kleeman, R.: Rectification of the Madden–Julian Oscillation into the ENSO Cycle, J. Clim., 13, 3560–3575, https://doi.org/10.1175/1520-0442(2000)013%3C3560:ROTMJO%3E2.0.CO;2, 2000.

Kiladis, G. N., Dias, J., Straub, K. H., Wheeler, M. C., Tulich, S. N., Kikuchi, K., Weickmann, K. M., and Ventrice, M. J.: A Comparison of OLR and Circulation-Based Indices for Tracking the MJO, Mon. Weather Rev., 142, 1697–1715, https://doi.org/10.1175/MWR-D-13-00301.1, 2014.

Kim, D., Sperber, K., Stern, W., Waliser, D., Kang, I.-S., Maloney, E., Wang, W., Weickmann, K., Benedict, J., Khairoutdinov, M., Lee, M.-I., Neale, R., Suarez, M., Thayer-Calder, K., and Zhang, G.: Application of MJO Simulation Diagnostics to Climate Models, J. Clim., 22, 6413–6436, https://doi.org/10.1175/2009JCLI3063.1, 2009.

Kim, H., Vitart, F., and Waliser, D. E.: Prediction of the Madden–Julian Oscillation: A Review, J. Clim., 31, 9425–9443, https://doi.org/10.1175/JCLI-D-18-0210.1, 2018.

Kim, H.-M., Kim, D., Vitart, F., Toma, V. E., Kug, J.-S., and Webster, P. J.: MJO Propagation across the Maritime Continent in the ECMWF Ensemble Prediction System, J. Clim., 29, 3973–3988, https://doi.org/10.1175/JCLI-D-15-0862.1, 2016.

Kim, H.-R., Ha, K.-J., Roxy, M. K., Chung, E.-S., Wang, B., Lee, S.-S., and Moon, J.-Y.: Recent asymmetric tropical ocean warming has altered regional propagation of Madden-Julian Oscillation, Commun. Earth Environ., 6, 663, https://doi.org/10.1038/s43247-025-02652-z, 2025.

Klingaman, N. P. and Woolnough, S. J.: The role of air–sea coupling in the simulation of the Madden–Julian oscillation in the Hadley Centre model, Q. J. R. Meteorol. Soc., 140, 2272–2286, https://doi.org/10.1002/qj.2295, 2014.

Kociuba, G. and Power, S. B.: Inability of CMIP5 Models to Simulate Recent Strengthening of the Walker Circulation: Implications for Projections, J. Clim., 28, 20–35, https://doi.org/10.1175/JCLI-D-13-00752.1, 2015.

Leyva, I., Martínez, J. H., Masoller, C., Rosso, O. A., and Zanin, M.: 20 years of ordinal patterns: Perspectives and challenges, Europhys. Lett., 138, 31001, https://doi.org/10.1209/0295-5075/ac6a72, 2022.

https://doi.org/10.5194/egusphere-2026-3251
Preprint. Discussion started: 23 June 2026

Liebmann, B. and Smith, C. A.: Description of a complete (interpolated) outgoing longwave radiation dataset, Bull. Am. Meteorol. Soc., 77, 1275–1277, 1996.

Liu, P., Zhang, Q., Zhang, C., Zhu, Y., Khairoutdinov, M., Kim, H.-M., Schumacher, C., and Zhang, M.: A revised real-time multivariate MJO index, Mon. Weather Rev., 144, 627–642, https://doi.org/10.1175/MWR-D-15-0237.1, 2016.

Lyu, M., Jiang, X., and Wu, Z.: A Cautionary Note on the Long-term Trend in Activity of the Madden-Julian Oscillation During the Past Decades, Geophys. Res. Lett., 46, 14063–14071, https://doi.org/10.1029/2019GL086133, 2019.

Madden, R. A. and Julian, P. R.: Detection of a 40–50 Day Oscillation in the Zonal Wind in the Tropical Pacific, J. Atmospheric Sci., 28, 702–708, https://doi.org/10.1175/1520-0469(1971)028%3C0702:DOADOI%3E2.0.CO;2, 1971.

Maloney, E. D., Adames, Á. F., and Bui, H. X.: Madden–Julian oscillation changes under anthropogenic warming, Nat. Clim. Change, 9, 26–33, https://doi.org/10.1038/s41558-018-0331-6, 2019.

Merryfield, W. J., Baehr, J., Batté, L., Becker, E. J., Butler, A. H., Coelho, C. A. S., Danabasoglu, G., Dirmeyer, P. A., Doblas-Reyes, F. J., Domeisen, D. I. V., Ferranti, L., Ilynia, T., Kumar, A., Müller, W. A., Rixen, M., Robertson, A. W., Smith, D. M., Takaya, Y., Tuma, M., Vitart, F., White, C. J., Alvarez, M. S., Ardilouze, C., Attard, H., Baggett, C., Balmaseda, M. A., Beraki, A. F., Bhattacharjee, P. S., Bilbao, R., De Andrade, F. M., DeFlorio, M. J., Díaz, L. B., Ehsan, M. A., Fragkoulidis, G., Gonzalez, A. O., Grainger, S., Green, B. W., Hell, M. C., Infanti, J. M., Isensee, K., Kataoka, T., Kirtman, B. P., Klingaman, N. P., Lee, J.-Y., Mayer, K., McKay, R., Mecking, J. V., Miller, D. E., Neddermann, N., Justin Ng, C. H., Ossó, A., Pankatz, K., Peatman, S., Pegion, K., Perlwitz, J., Recalde-Coronel, G. C., Reintges, A., Renkl, C., Solaraju-Murali, B., Spring, A., Stan, C., Sun, Y. Q., Tozer, C. R., Vigaud, N., Woolnough, S., and Yeager, S.: Current and Emerging Developments in Subseasonal to Decadal Prediction, Bull. Am. Meteorol. Soc., 101, E869–E896, https://doi.org/10.1175/BAMS-D-19-0037.1, 2020.

Miura, H., Satoh, M., Nasuno, T., Noda, A. T., and Oouchi, K.: A Madden-Julian Oscillation Event Realistically Simulated by a Global Cloud-Resolving Model, Science, 318, 1763–1765, https://doi.org/10.1126/science.1148443, 2007.

Mogensen, K., Keeley, S., and Towers, P.: Coupling of the NEMO and IFS models in a single executable, https://doi.org/10.21957/RFPLWZUOL, 2012.

https://doi.org/10.5194/egusphere-2026-3251
Preprint. Discussion started: 23 June 2026

North, G. R., Bell, T. L., Cahalan, R. F., and Moeng, F. J.: Sampling Errors in the Estimation of Empirical Orthogonal Functions, Mon. Weather Rev., 110, 699–706, https://doi.org/10.1175/1520-0493(1982)110%3C0699:SEITEO%3E2.0.CO;2, 1982.

Oliver, E. C. J. and Thompson, K. R.: A Reconstruction of Madden–Julian Oscillation Variability from 1905 to 2008, J. Clim., 25, 1996–2019, https://doi.org/10.1175/JCLI-D-11-00154.1, 2011.

Pohl, B. and Matthews, A. J.: Observed Changes in the Lifetime and Amplitude of the Madden–Julian Oscillation Associated with Interannual ENSO Sea Surface Temperature Anomalies, J. Clim., 20, 2659–2674, https://doi.org/10.1175/JCLI4230.1, 2007.

Power, S., Lengaigne, M., Capotondi, A., Khodri, M., Vialard, J., Jebri, B., Guilyardi, E., McGregor, S., Kug, J.-S., Newman, M., McPhaden, M. J., Meehl, G., Smith, D., Cole, J., Emile-Geay, J., Vimont, D., Wittenberg, A. T., Collins, M., Kim, G.-I., Cai, W., Okumura, Y., Chung, C., Cobb, K. M., Delage, F., Planton, Y. Y., Levine, A., Zhu, F., Sprintall, J., Di Lorenzo, E., Zhang, X., Luo, J.-J., Lin, X., Balmaseda, M., Wang, G., and Henley, B. J.: Decadal climate variability in the tropical Pacific: Characteristics, causes, predictability, and prospects, Science, 374, eaay9165, https://doi.org/10.1126/science.aay9165, 2021.

Rashid, H. A., Hendon, H. H., Wheeler, M. C., and Alves, O.: Prediction of the Madden–Julian oscillation with the POAMA dynamical prediction system, Clim. Dyn., 36, 649–661, https://doi.org/10.1007/s00382-010-0754-x, 2011.

Roberts, C. D., Keeley, S., Mogensen, K., Pelletier, C., and Zuo, H.: The role of the oceans for subseasonal prediction: insights from eddy-permitting and eddy-rich coupled forecast systems, https://doi.org/10.48550/arXiv.2605.00621, 1 May 2026.

Roundy, P. E.: On the Interpretation of EOF Analysis of ENSO, Atmospheric Kelvin Waves, and the MJO, J. Clim., 28, 1148–1165, https://doi.org/10.1175/JCLI-D-14-00398.1, 2015.

Roundy, P. E., Schreck, C. J., and Janiga, M. A.: Contributions of Convectively Coupled Equatorial Rossby Waves and Kelvin Waves to the Real-Time Multivariate MJO Indices, Mon. Weather Rev., 137, 469–478, https://doi.org/10.1175/2008MWR2595.1, 2009.

Shannon, C. E.: A Mathematical Theory of Communication, Bell Syst. Tech. J., 27, 379–423, https://doi.org/10.1002/j.1538-7305.1948.tb01338.x, 1948.

https://doi.org/10.5194/egusphere-2026-3251
Preprint. Discussion started: 23 June 2026

Stachnik, J. P. and Chrisler, B.: An Index Intercomparison for MJO Events and Termination, J. Geophys. Res. Atmospheres, 125, e2020JD032507, https://doi.org/10.1029/2020JD032507, 2020.

Stan, C., Straus, D. M., Frederiksen, J. S., Lin, H., Maloney, E. D., and Schumacher, C.: Review of Tropical-Extratropical Teleconnections on Intraseasonal Time Scales, Rev. Geophys., 55, 902–937, https://doi.org/10.1002/2016RG000538, 2017.

Stan, C., Zheng, C., Chang, E. K.-M., Domeisen, D. I. V., Garfinkel, C. I., Jenney, A. M., Kim, H., Lim, Y.-K., Lin, H., Robertson, A., Schwartz, C., Vitart, F., Wang, J., and Yadav, P.: Advances in the Prediction of MJO Teleconnections in the S2S Forecast Systems, Bull. Am. Meteorol. Soc., 103, E1426–E1447, https://doi.org/10.1175/BAMS-D-21-0130.1, 2022.

Suematsu, T. and Miura, H.: Changes in the Eastward Movement Speed of the Madden–Julian Oscillation with Fluctuation in the Walker Circulation, J. Clim., 35, 211–225, https://doi.org/10.1175/JCLI-D-21-0269.1, 2022.

Suematsu, T., Miura, H., Kodama, C., and Takasuka, D.: Deceleration of Madden–Julian Oscillation Speed in NICAM AMIP-Type Simulation Associated With Biases in the Walker Circulation Strength, Geophys. Res. Lett., 49, e2022GL098628, https://doi.org/10.1029/2022GL098628, 2022.

Taraphdar, S., Zhang, F., Leung, L. R., Chen, X., and Pauluis, O. M.: MJO Affects the Monsoon Onset Timing Over the Indian Region, Geophys. Res. Lett., 45, 10011–10018, https://doi.org/10.1029/2018GL078804, 2018.

Vancoppenolle, M., Rousset, C., Blockley, E., Aksenov, Y., Feltham, D., Fichefet, T., Garric, G., Guémas, V., Iovino, D., Keeley, S., Madec, G., Massonnet, F., Ridley, J., Schroeder, D., and Tietsche, S.: SI3, the NEMO Sea Ice Engine, https://doi.org/10.5281/ZENODO.7534899, 2023.

Ventrice, M. J., Wheeler, M. C., Hendon, H. H., Schreck, C. J., Thorncroft, C. D., and Kiladis, G. N.: A Modified Multivariate Madden–Julian Oscillation Index Using Velocity Potential, Mon. Weather Rev., 141, 4197–4210, https://doi.org/10.1175/MWR-D-12-00327.1, 2013.

Vitart, F.: Madden—Julian Oscillation prediction and teleconnections in the S2S database, Q. J. R. Meteorol. Soc., 143, 2210–2220, https://doi.org/10.1002/qj.3079, 2017.

Waliser, D.: MJO Simulation Diagnostics, J. Clim., 22, 3006–3030, https://doi.org/10.1175/2008JCLI2731.1, 2009.

https://doi.org/10.5194/egusphere-2026-3251
Preprint. Discussion started: 23 June 2026

Weidman, S., Kleiner, N., and Kuang, Z.: A Rotation Procedure to Improve Seasonally Varying Empirical Orthogonal Function Bases for MJO Indices, Geophys. Res. Lett., 49, e2022GL099998, https://doi.org/10.1029/2022GL099998, 2022.

Weller, E., Min, S.-K., Cai, W., Zwiers, F. W., Kim, Y.-H., and Lee, D.: Human-caused Indo-Pacific warm pool expansion, Sci. Adv., 2, e1501719, https://doi.org/10.1126/sciadv.1501719, 2016.

Wheeler, M. and Kiladis, G. N.: Convectively Coupled Equatorial Waves: Analysis of Clouds and Temperature in the Wavenumber–Frequency Domain, J. Atmospheric Sci., 56, 374–399, https://doi.org/10.1175/1520-0469(1999)056%3C0374:CCEWAO%3E2.0.CO;2, 1999.

Wheeler, M. C. and Hendon, H. H.: An All-Season Real-Time Multivariate MJO Index: Development of an Index for Monitoring and Prediction, Mon. Weather Rev., 132, 1917–1932, https://doi.org/10.1175/1520-0493(2004)132%3C1917:AARMMI%3E2.0.CO;2, 2004.

Wheeler, M. C., Hendon, H. H., Cleland, S., Meinke, H., and Donald, A.: Impacts of the Madden–Julian Oscillation on Australian Rainfall and Circulation, J. Clim., 22, 1482–1498, https://doi.org/10.1175/2008JCLI2595.1, 2009.

Yadav, P., Garfinkel, C. I., and Domeisen, D. I. V.: The Role of the Stratosphere in Teleconnections Arising From Fast and Slow MJO Episodes, Geophys. Res. Lett., 51, e2023GL104826, https://doi.org/10.1029/2023GL104826, 2024.

Yoo, C., Feldstein, S., and Lee, S.: The impact of the Madden-Julian Oscillation trend on the Arctic amplification of surface air temperature during the 1979-2008 boreal winter: IMPACT OF MJO ON POLAR AMPLIFICATION, Geophys. Res. Lett., 38, n/a-n/a, https://doi.org/10.1029/2011GL049881, 2011.

Zhang, C.: Madden-Julian Oscillation, Rev. Geophys., 43, 2004RG000158, https://doi.org/10.1029/2004RG000158, 2005.

Zhao, C., Ren, H.-L., Song, L., and Wu, J.: Madden–Julian Oscillation simulated in BCC climate models, Dyn. Atmospheres Oceans, 72, 88–101, https://doi.org/10.1016/j.dynatmoce.2015.10.004, 2015.

Zwiers, F. W. and Von Storch, H.: Taking Serial Correlation into Account in Tests of the Mean, J. Clim., 8, 336–351, https://doi.org/10.1175/1520-0442(1995)008%3C0336:TSCIAI%3E2.0.CO;2, 1995.